HYDROGEN PRODUCTION BY PHOTOELECTROLYTIC DECOMPOSITION OF H_2O USING SOLAR ENERGY

FINAL REPORT

December 1, 1978 - November 30, 1979

R. D. Rauh
S. A. Alkaitis
J. M. Buzby
R. Schiff

EIC Corporation
55 Chapel Street
Newton, Massachusetts 02158

August, 1980

Prepared for

CALIFORNIA INSTITUTE OF TECHNOLOGY
JET PROPULSION LABORATORY
4800 Oak Grove Drive
Pasadena, California 91103

UNDER CONTRACT NO. 955271

This work was performed for the Jet Propulsion Laboratory, California Institute of Technology sponsored by the National Aeronautics and Space Administration under CONTRACT NAS7-100.

HYDROGEN PRODUCTION BY PHOTOELECTROLYTIC DECOMPOSITION OF H_2O USING SOLAR ENERGY

FINAL REPORT

December 1, 1978 - November 30, 1979

R. D. Rauh
S. A. Alkaitis
J. M. Buzby
R. Schiff

EIC Corporation
55 Chapel Street
Newton, Massachusetts 02158

August, 1980

Prepared for

CALIFORNIA INSTITUTE OF TECHNOLOGY
JET PROPULSION LABORATORY
4800 Oak Grove Drive
Pasadena, California 91103

UNDER CONTRACT NO. 955271

This work was performed for the Jet Propulsion Laboratory, California Institute of Technology sponsored by the National Aeronautics and Space Administration under CONTRACT NAS7-100.

ABSTRACT

The goal of this program is to develop photoelectrochemical systems for the efficient decomposition of water. The work is directed toward three aspects of this problem:

- Synthesis and Evaluation of New Photoanodes. Semiconducting d-band oxides have been sought, which would yield the combination of stability, low electron affinity, and moderate band gap essential for an efficient photoanode. Of over 150 mixed transition metal oxides investigated on this program, PdO and $Fe_{2-x}Rh_xO_3$ appear most likely to fulfill the stated goals. Oxygen evolution yields may also be improved by mediation of high energy oxidizing agents, such as CO_3^-.

- Examination of Photocathodes. Examination of several p-type semiconductors as photocathodes revealed remarkable stability for p-GaAs, and also indicated p-CdTe as a stable H_2 photoelectrode.

- Photoelectrochemical System Evaluation. Several potentially economical schemes for photoelectrochemical decomposition of water were examined, including photoelectrochemical diodes and two-stage, four-photon processes. These concepts were demonstrated for systems based on platinized $SiTiO_3$ (H_2O decomposition), platinized CdS (H_2S decomposition), and a CdS/Fe_2O_3 dual photoelectrode cell.

TABLE OF CONTENTS

LIST OF FIGURES

LIST OF FIGURES
(Continued)

LIST OF TABLES

I. INTRODUCTION

The purpose of this program is to design, fabricate and test semiconducting electrodes for the photoelectrolysis of water with the concurrent evaluation of photoelectrolyzer configurations. The ultimate goal is the direct, efficient and practical conversion of solar energy into a storable, transportable fuel, namely hydrogen.

Our overall research schedule for this program is focused on three principal areas of investigation:

1. The synthesis and evaluation of new photoanodes.
2. The synthesis and evaluation of new photocathodes.
3. Evaluation of photoelectrolyzer configurations.

Band energetics are all-important in the design of photoelectrodes. Briefly, the electron affinity (EA) and the band gap (ΔE_g) determine to first order the energetic positions of the conduction and valence bands (E_c, E_v) relative to the redox species in solution. The interfacial band energies may be further modified by adsorbed neutral or ionizable surface groups. Experimentally, the band positions of a semiconductor at an aqueous interface may be placed relative to the H^+/H_2 and O_2/H_2O redox energy levels by a combined measurement of the flat band potential (V_{fb}) vs. a standard reference electrode and the band gap (ΔE_g).

A single photoelectrode configuration operating spontaneously (Class I photoelectrode) requires a semiconductor whose surface values of E_v and E_c straddle the O_2/H_2O and H^+/H_2 redox levels. This is true whether the semiconductor electrode is an anode (n-type) or a cathode (p-type). For a dual photoelectrode cell or a single one operating with an external bias (Class II photoelectrode), the p-side must have its E_c <u>above</u> the H^+/H_2 energy, while the n-side must have its E_v <u>below</u> the O_2/H_2O energy, and there must be some overlap between their band gaps. These energetic differences between bands and redox levels must also be sufficient to accommodate the band bending and overpotentials necessary to separate light produced carriers and drive the electron transfer reactions, respectively.

There have been no photoelectrodes (photoanodes) yet demonstrated which meet both the criteria of V_{fb} and ΔE_g necessary for practical Class I or Class II photoelectrodes. The realistic lower limit for the ΔE_g of a Class I material would be $\sim$1.8 eV whereas a Class II material could have a ΔE_g in the range 0.9-1.8 eV, since it need only provide half the energy for H_2O decomposition. Of the known stable Class I semiconductors, all are n-type oxides and all have band gaps in excess of 3 eV. Similarly,

of the known stable Class II materials, most have band gaps >2 eV, and if ΔE_g is smaller, then the V_{fb} and the ΔE_g requirements are barely met.

In order to have a metal oxide with both low EA and ΔE_g, it may be possible to interpose a band of nonbonding d-electron parentage within the band gap. An ongoing aspect of our research is the attempt to produce photoresponsive, n-type "d-band" oxide photoanodes (1,2). This is to be achieved through the introduction of d^n metal oxides into the lattices of d^o, Class I photoanodes. To date, this approach has been most successful with $4d^n$ and $5d^n$ metals. Collective electron behavior, or band formation, is more likely than with $3d^n$ metals, due to the greater radial distribution of the 4d and 5d electrons.

One question regarding photoanode operation is the effect of the excess hole energy on the mechanism of O_2 evolution. It has been demonstrated by us as well as by Gerstner and co-workers (3) that addition of high energy redox couples to the electrolyte can alter this mechanism and in some cases enhance the overall kinetics of electron transfer. Similarly, the rate of O_2 evolution can be affected by the ability of the electrode surface to stabilize intermediates such as OH or O.

In Section II of this report, results of our continued research on d-band oxide photoanodes are reviewed, with emphasis on 4d and 5d cations. Section III summarizes research on photoelectrochemical diode structures. Section IV summarizes research on p-type photocathodes for photoelectrochemical H_2 production. In Section V we consider some systems which could be employed as the bases for economical solar fuel producing devices, and show preliminary experimental results for several such alternatives.

II. PHOTOANODE DEVELOPMENT

The problem of developing a low electron affinity, low band gap semiconducting oxide has been described in our First Annual Report (1) and in a related publication (2). An investigation by us of over 50 perovskite and rutile based oxides was carried out to determine the effects of photoelectrochemical properties of adding d^n transition metals to the lattice of $MTi^{+4}O_3$ or TiO_2. Our results on this initial series of oxides indicated that the d^n ions could indeed act as centers for photocurrent sensitized by visible light. However, in most cases they also acted as traps for optically produced minority carriers, diminishing the overall efficiency of photocurrent production.

During the past year we have continued our survey of mixed metal oxide photoanodes. Parent compounds under investigation are TiO_2, $BaTiO_3$ and Fe_2O_3. For the most part, solutions of these materials with the Pt group 4d and 5d metals were studied, as the latter have large d orbital radii and could show the greatest tendency to collective d electron behavior.

A. Experimental Procedures

1. Photoelectrochemical Measurements

Our procedures for phase-sensitive photoelectrochemical measurements have been described previously (1,2). The measurements of the photoresponse of the photoelectrodes as a function of the exciting wavelength had been previously limited to only the strongest responding electrodes when using monochromated light due to the high noise level in the system. For weaker and/or slower responding electrodes, only integrated photoresponse could be obtained using cutoff filters. The noise problem prevented the estimation of the band gaps of these electrodes from a measurement of photoresponse versus wavelength due to the very low intensity of the monochromatic light needed for these measurements. A large part of this problem has been traced to the Wenking LT73 potentiostat. We have alleviated this problem by designing and building a new noise-free battery powered potentiostat whose circuit diagram is shown in Figure 1.

2. Synthesis of Oxide Photoelectrodes

Photoelectrodes were prepared as sintered polycrystalline pellets and as thin films deposited on platinum and sintered polycrystalline pellet substrates. The compounds synthesized and evaluated photoelectrochemically are listed in Table 1. The synthetic procedures for the preparation of polycrystalline pellets were outlined in the First Annual Report (1). Briefly, component oxides and/or nitrates and/or carbonates were thoroughly mixed, sintered once, then ground and thoroughly mixed again, pressed into pellets using polyvinyl alcohol as a binder and sintered for a final time.

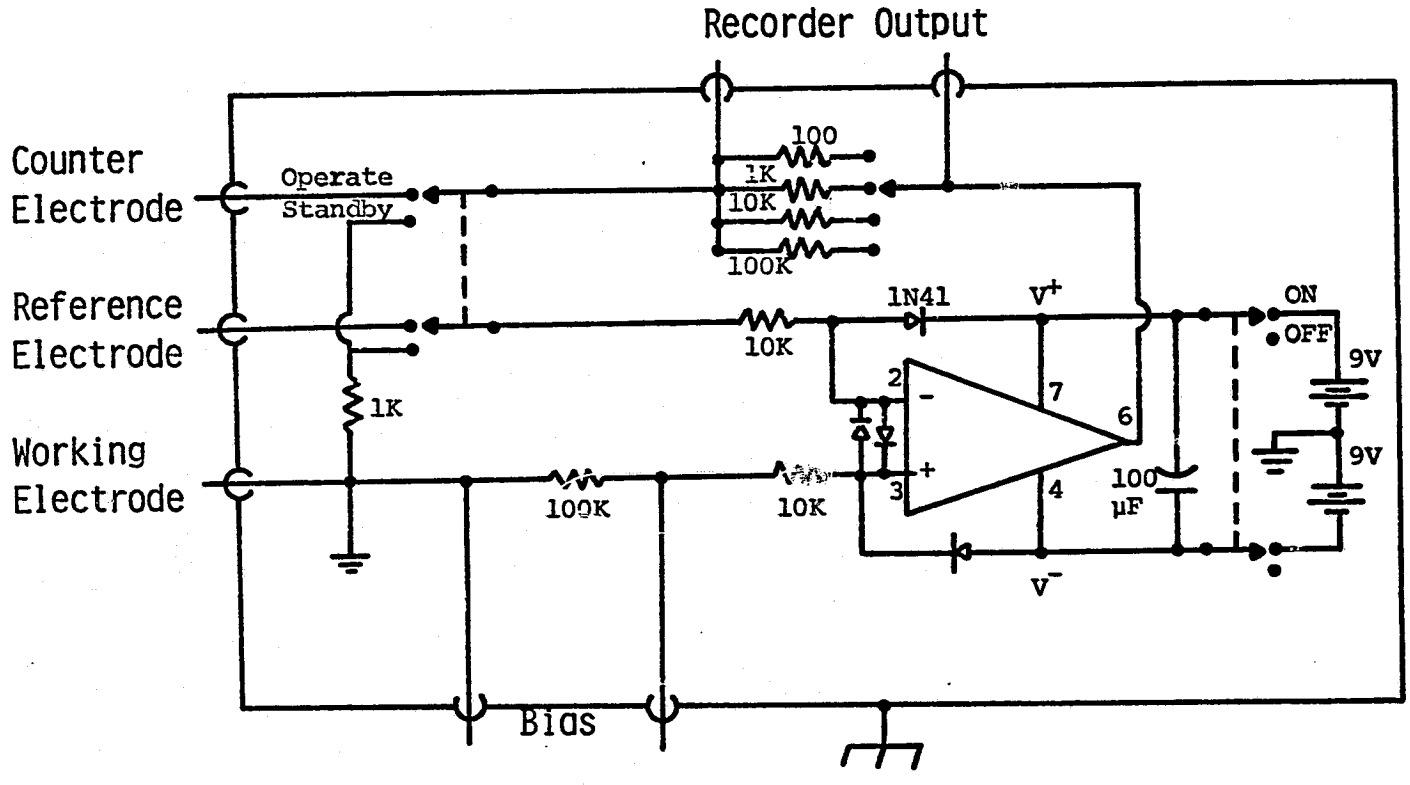

Fig. 1: Schematic of low noise potentiostat. All input and output connectors are BNC jacks. Input impedance, Z_{in}, is $10^{12}\Omega$ for the reference electrode. Maximum output current is 5 mA on 100 or 1KΩ setting, 500 µA on 10KΩ, and 50 µA on 100KΩ.

TABLE 1

SYNTHESIS OF MIXED OXIDE PHOTOELECTRODES

Photoelectrode Composition	Code	Initial Sinter[a] Temp. (°C)	Initial Sinter[a] Time (hr)	Final Sinter[a,b] Temp. (°C)	Final Sinter[a,b] Time (hr)	Ref.
	Corundum Structure					
$Fe_2O_3 \cdot 0.02TiO_2$		900	18	1350	8	
$Fe_2O_3 \cdot 0.11Al_2O_3 \cdot 0.022TiO_2$	F-24	900	20	1400	8	
$Fe_2O_3 \cdot 0.25Al_2O_3 \cdot 0.05TiO_2$	F-25	900	20	1400	8	
$(Fe_{1-x}Rh_x)_2O_2$	c					a
	Spinel Structure					
Ni_2TiO_4	L-5	1200	20	1400	12	
$NiFe_2O_4$	L-7	900	20	1300	8	b,c
$ZnFe_{1.98}Ti_{0.02}O_4$	S-3	900	20	1200[d]	8	c
$BaFe_{11.88}Ti_{0.12}O_{19}$	S-4	900	20	1300	8	d
$Co_{0.93}Fe_{2.07}O_4$	S-5	900	20	1300	8	e
$CdIn_2O_4$	S-7	c				f
	Rutile Structure					
$Ti_6Cr_2O_{15}$	T-51	1100/1300	20/75	1300	75	g
$Ti_7Cr_2O_{17}$	T-52	1100/1300	20/75	1300	75	g
$Ti_8Cr_2O_{19}$	T-53	1100/1300	20/75	1300	75	g
$Ti_9Cr_2O_{21}$	T-54	1100/1300	20/75	1300	75	g
$Ti_{12}Cr_2O_{27}$	T-55	1100/1300	20/75	1300	75	g
	Perovskite Structure					
$YceFeNiO_6$	L-4	1200	20	1400	12	

[a] In air.
[b] Samples in form of pellets.
[c] Thin films, formed in a flame.
[d] Subsequently sintered at 1250°C for 3 hr.

References

a. J. M. D. Coey and G. A. Sawatzky, J. Phys., 4C, 2386 (1971).
b. L. G. Van Uitert, J. Chem. Phys., 24, 306 (1956).
c. Ibid., 23, 1883 (1955).
d. H. J. Van Hook, J. Am. Cer. Soc., 47, 579 (1964).
e. G. H. Jonker, J. Phys. Chem. Solids, 9, 165 (1959).
f. V. O. Schmitz-DuMont and H. Kasper, Z. Anorg. Chem., 341, 252 (1965).
g. S. Andersson, A. Sundholm and A. Magneli, Acta Chem. Scand., 13, 989 (1969).

The new n-type photoelectrode, $CdIn_2O_4$, a spinel, was prepared as a thin film on a platinum substrate by evaporation of an aqueous solution containing 0.05M $Cd(NO_3)_2$ and 0.1M $InCl_3$ and heating the platinum to ~600°C. Mixtures of iron oxide and rhodium oxide, $(Fe_{1-x}Rh_x)_2O_3$, with x = 0.05, 0.1, 0.125, 0.25 and 0.5 were also synthesized as thin films on platinum and sintered $Fe_2O_3 \cdot 0.02TiO_2$ pellet substrates. Coey and Sawatzky have shown (4) that a complete range of solid solutions of Rh_2O_3 in Fe_2O_3 can be obtained while maintaining the corundum structure of αFe_2O_3. The following physical properties of Rh_2O_3 precluded the formation of sintered polycrystalline pellets:

a. Rh_2O_3 decomposes to the metal at 1130°C at 1 atm O_2 pressure (5).

b. αRh_2O_3 (corundum structure) undergoes an irreversible structural change in the temperature range of 750-1000°C (5,6).

The photoelectrodes were prepared by evaporating aqueous solutions of $Fe(NO_3)_3 \cdot 9H_2O$ and $Rh(NO_3)_3 \cdot 2H_2O$, 10^{-3}M in HNO_3 and 0.1M in $Fe^{+3} + Rh^{+3}$, on a platinum substrate, decomposing the nitrates at $T \leq 500$°C and sintering the electrodes in air for 20 hours at 900°C (1). Homogeneity of the films was improved by the addition of a drop of methanol during the initial evaporation of the aqueous Fe^{+3}-Rh^{+3} solutions on the platinum. The procedures used to synthesize the same series of compounds on $Fe_2O_3 \cdot 0.02$ TiO_2 pellets as a substrate were similar. The polycrystalline Fe_2O_3 (1 atom % TiO_2) pellets were prepared by sintering intimate mixtures of Fe_2O_3 and TiO_2 in air at 1300-1350°C for 20 hours. Appropriate mixtures of 10^{-1}M $Fe(NO_3)_3 \cdot 9H_2O$ and 10^{-1}M $Rh(NO_3)_3 \cdot 2H_2O$, both in 10^{-3}M HNO_3, were then evaporated on one face of the iron oxide pellets. The nitrates were then decomposed at about 500°C in a flame (this process repeated 5 times per pellet), and the coated pellets sintered in air at 900°C for 3 days.

3. Measurement of Flat Band Potential (V_{fb}) and Band Gap (ΔE_g)

Flat band potentials and band gaps of the photoelectrodes were determined according to procedures outlined by Butler (7). He has shown that for wide band gap semiconductors, the semiconductor properties and not the electrode kinetics are the crucial characteristics in determining photoresponse. Under these conditions, the semiconductor-electrolyte interface can be treated as a Schottky barrier and the photocurrent described by

$$J = q\phi_o \left(1 - \frac{\exp[\alpha W_o (V - V_{fb})^{\frac{1}{2}}]}{1 + \alpha L_p} \right), \qquad (1)$$

where J is the photocurrent, q is the electronic charge, ϕ_o is the photon flux, α is the optical absorption, W_o is the characteristic depletion

layer width, V is the applied potential and V_{fb} is the flat band potential both relative to the same reference, and L_p is the hole diffusion length. It also has been shown that the optical absorption for interband transitions close to the semiconductor's band gap behaves as:

$$\alpha = A(h\nu-\Delta E_g)^{n/2}/h\nu \qquad (2)$$

where A is a constant, ΔE_g is the band gap, and n is a function of whether the transition is direct (n=1) or indirect (n=4). Considering absorption close to the band gap, $\alpha L_p << 1$ and $2W_o << 1$. Expanding the exponential for $\alpha W_o << 1$, we get

$$\frac{J}{q\phi_o} = \frac{A(h\nu-\Delta E_g)^{n/2}}{h\nu}\,\alpha W_o (V-V_{fb})^{\frac{1}{2}} \qquad (3)$$

For indirect transitions (n=4), a plot of $(Jh\nu)^{\frac{1}{2}}$ vs. $h\nu$ will give a straight-line whose intercept will be ΔE_g of the semiconductor. Such a plot is shown in Figure 2 for $CdIn_2O_4$ and the ΔE_g = 2.33 eV. ΔE_g as determined from the onset of photocurrent is also 2.3 eV. Choosing a wavelength close to the band gap, the photocurrent then should vary with the applied potential as

$$V-V_{fb} \sim \left(J/\alpha W_o q\phi_o\right)^2 \qquad (4)$$

and a plot of J^2 vs. V (applied potential) should be linear with an intercept of V_{fb}. Such a plot is shown in Figure 2 also for $CdIn_2O_4$. The flat band potential is -0.6 at pH = 13.

B. Platinum Metal Substituted $BaTiO_3$ Photoanodes

A particularly interesting group of photoanodes may be the $BaTi_{1-x}M_xO_3$ compounds, where M is a group VIII metal. These compounds are known to form a continuous series for many metal substituents (8). Structural evidence shows that addition of a d^n metal induces a hexagonal distortion in the parent perovskite, which is a result of enhanced metal-metal bonding. This effect could give rise to d band formation in the mixed metal oxides.

Single crystals of the $BaTi_{1-x}M_xO_3$ series have been produced by Matthias (9) employing slow crystallization from a molten carbonate flux. Several unsuccessful attempts to grow such crystals were made in the present work. Stoichiometric mixtures of $BaCO_3$, TiO_2 and the Pt metal oxide were initially incorporated into a $BaCl_2$ flux, heated to 1100°C (10), and cooled at a rate of 3%/hr. However, no crystals were obtained. We also tried pre-synthesizing powders of $BaTi_{2/3}M_{1/3}O_3$, M = Ru, Rh, and Pd and $BaTi_{0.9}Pt_{0.1}O_3$ by sintering stoichiometric

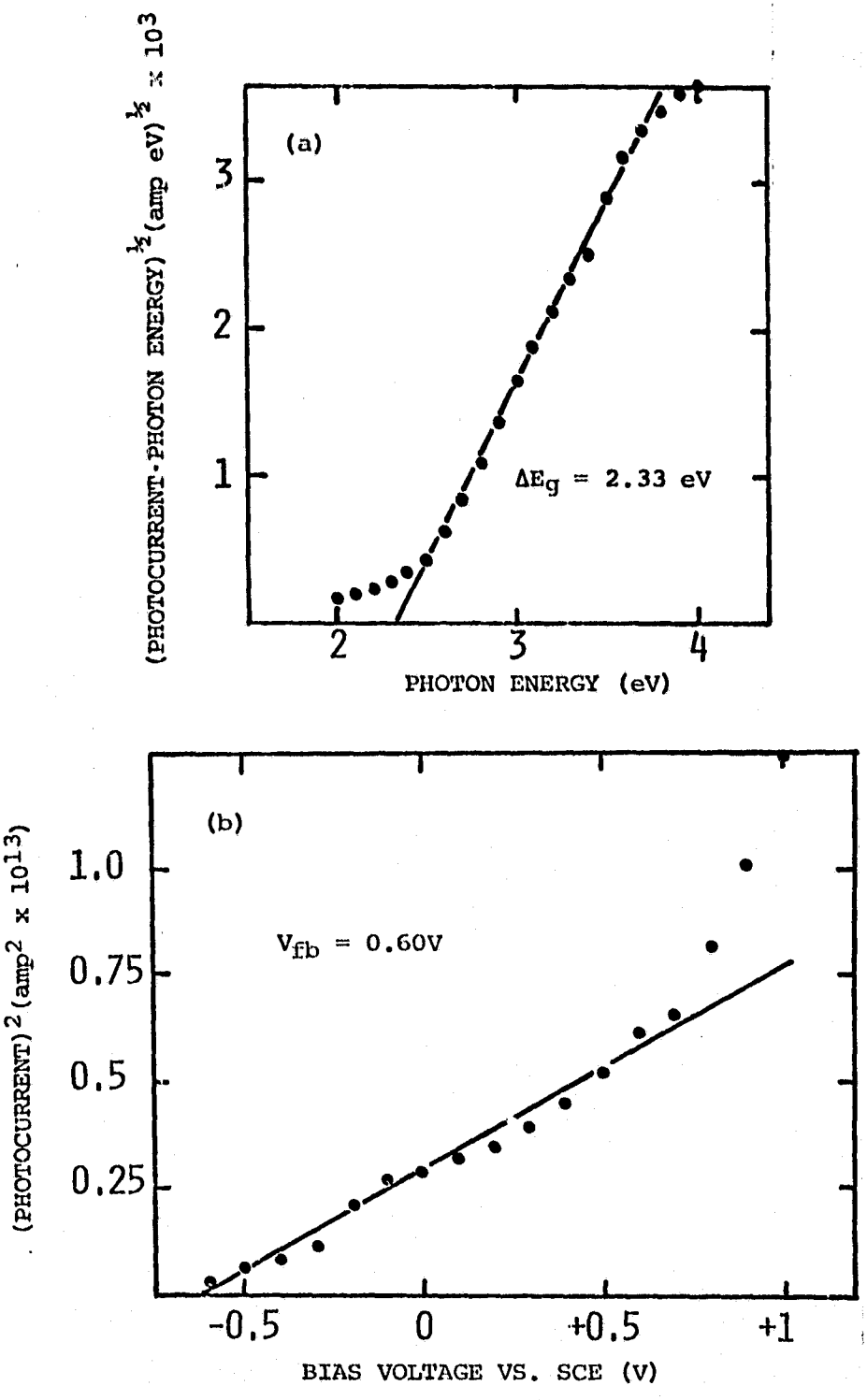

Fig. 2: Band gap (ΔE_G) and flat band potential (V_{fb}) determination for thin film $CdIn_2O_4$ photoelectrodes. Solutions were adjusted to pH = 13 with NaOH.

mixtures of $BaCO_3$, TiO_2 and the metal oxides (Ru, Rh and Pt) or metals (Pd) at 700°C and 900°C in air for 24 hours at each temperature. The sintered powders were then mixed with $BaCl_2$ (5-8 moles $BaCl_2$ per mole of powder), soaked at 1100°C for 6 hours, and slowly cooled at 3°C/hr to 800°C. Again, no crystals appeared. Varying experimental parameters also did not result in the production of any single crystals.

As an immediate alternative, we made sintered polycrystalline pellets of the above compounds. Three sintering cycles were employed: 700°C, 900°C, and 1250°C. The compounds with M = Ru and Rh did not react very well, but the pellets were tested nevertheless. Both gave large dark currents, photocurrents of $\sim$0.5 mA/cm^2 with rather positive flat band potentials and had slow photoresponses. Another sintering cycle of 2.5 days at 1250°C did not improve the pellets. Synthesis at higher temperatures is rather difficult, since there is a tendency to produce metallic Ru and Rh. Both the Pd and Pt compounds seemed to react rather well. Both had high resistivities and therefore required reduction, that of the Pt compound being difficult to control. The reduced compounds had negligible photoresponses.

At this point, we are not convinced of the microscopic homogeneity of these compounds, and more work is necessary to grow well-characterized single crystals. Solid state measurements of carrier transport properties in these crystals would be necessary to discover the true effects of Pt metal alloying on the semiconducting properties of the parent $BaTiO_3$. The results on the sintered pellets do, however, complete an earlier survey by us on $AA'MM'O_3$ perovskites. In general, with M = Ti, compounds with M = Fe^{+3} and Cr^{+3} show increased visible light photoresponse. When M' = $Mn^{+2/+3}$, Co^{+3}, Ni^{+2}, or the Pt metals, photoresponse is quenched and the compound becomes highly unstable to anodic dissolution.

C. Mixed Oxides of TiO_2 and Cr_2O_3

Inclusion of Cr^{+3} into TiO_2 has been demonstrated by us (1,2) and by others (11) to extend the onset of photoresponse from $\sim$400 nm well into the visible wavelength region. Previously, Ghosh and co-workers had observed this effect with very low "doping" levels of Cr^{+3} (<1 M/O). However, $TiO_2 \cdot xCr_2O_3$ forms a complete range of solid solutions, so that larger incorporations of Cr^{+3} are possible.

A series of chromium doped titanium oxides, $Ti_{n-2}Cr_2O_{2n-1}$, were synthesized with n = 8, 9, 10, 11 and 14. Compound electrodes were prepared both as thin films and as polycrystalline sintered pellets. Thin films were prepared on platinum substrates by evaporating 7M HNO_3 solutions containing mixtures of $TiOCl_2$ and $Cr(NO_3)_3$ at a total concentration of 0.1M, and treating the electrode at red heat in a propane flame. This method, which yields quite sensitive films of TiO_2 itself, yielded films for the mixed oxides which had large dark currents and unstable photocurrents.

Sintered pellets could be produced with improved characteristics, although they appeared sensitive to the conditions of synthesis. Pellets were initially synthesized by sintering stoichiometric, finely ground mixtures of TiO_2 and Cr_2O_3 at 950°C for 20 hours. The sintered mass was reground, thoroughly mixed again, pressed into pellets using polyvinyl alcohol as a binder, then sintered at 1300°C for 75 hours. These electrodes also had unstable photocurrents and large dark currents. Stable photoelectrodes were finally prepared as polycrystalline pellets by employing three sintering cycles. The finely ground mixture was first sintered at 1100°C for 20 hours, reground, then sintered at 1300°C for 75 hours. Pellets fabricated from the doubly sintered material were then sintered at 1300°C for another 75 hours.

The photoelectrochemical characteristics of these electrodes are included in Table 2. The flat band potential (V_{fb}) decreases with increasing Cr concentration while the open circuit potential remains approximately constant. The photocurrents developed with full illumination from the Xe source are about half of that developed by TiO_2 under the same conditions. The action spectra indicate that the overall effect of chromium addition seems to be an increase in the far UV response, a lowering of the near UV response and the appearance of a tail extending into the visible. A very curious aspect of this system is the appearance of two distinct band gaps as shown in Figure 3. The band gap (ΔE_g) of $\approx$3 eV appears to be due to TiO_2, ΔE_g = 3.1 eV, whereas that of $\approx$2 eV appears to be due to Cr_2O_3. A possible explanation is that the chromium ions, which are arranged along crystal shear planes in these structures (4,5) produce localized intragap states. The $3d^3$ electrons of Cr^{+3} are necessarily localized since, if they were delocalized, a partially filled d-band would result giving the crystal metallic or semimetallic conductivity. Unsuccessful attempts were made to substitute Rh^{+3}, $4d^6$ (low spin), for some Cr^{+3} in thin film TiO_2-Cr_2O_3 photoelectrodes on platinum substrates.

TABLE 2

PHOTOELECTROCHEMICAL PROPERTIES OF MIXED Cr_2O_3-TiO_2 PHOTOELECTRODES

Electrode Material[a]	ΔE_g (eV)	V_{fb}[b]	Photocurrent[c] (mA/cm^2)
TiO_2	3.05	-0.7	1.42
$Ti_6Cr_2O_{15}$	2.94(2.05)	-0.5	0.97
$Ti_7Cr_2O_{17}$	3.0 (2.05)	-0.5	0.76
$Ti_8Cr_2O_{19}$	3.05(2.06)	-0.5	0.93
$Ti_9Cr_2O_{21}$	2.96(2.07)	-0.4	0.65
$Ti_{12}Cr_2O_{27}$	2.88(2.04)	-0.52	1.1

[a] Sintered polycrystalline pellets.
[b] Flat band potential versus SCE, pH = 10, 0.25M Na_2SO_4, 0.1M borate buffer.
[c] At +1V bias vs. SCE.

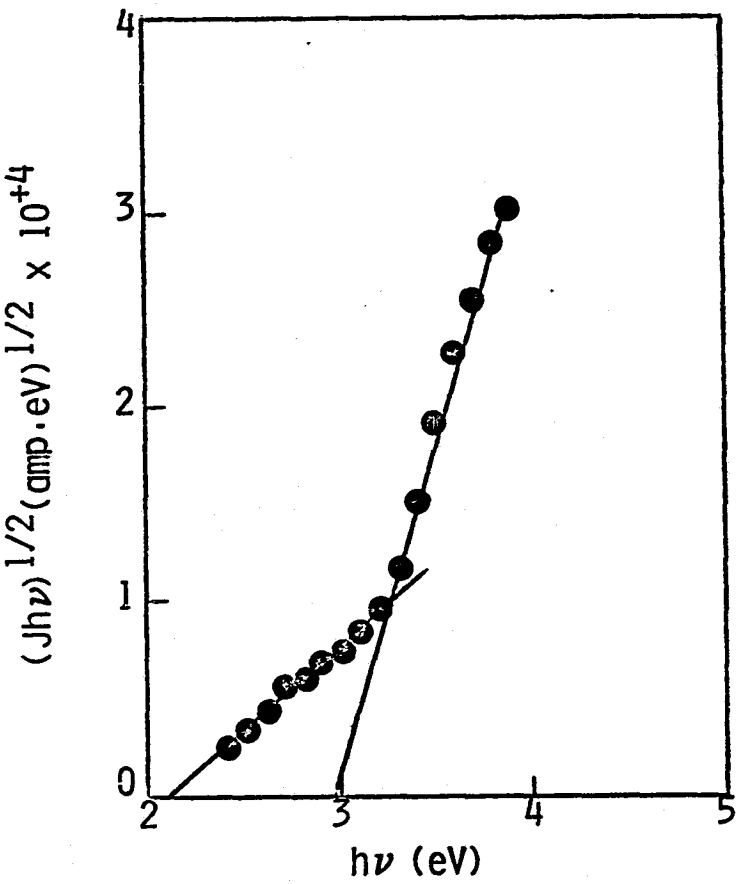

Fig. 3: Determination of the band gap for $Ti_9Cr_2O_{21}$ sintered polycrystalline photoelectrode.

D. Platinum Metal Oxide Doped Titanium Dioxide Photoelectrodes

We have extended our studies of chromium oxide doped titanium dioxide photoelectrodes to include the following platinum metal oxide dopants: RuO_2, Rh_2O_3, PdO, IrO_2 and PtO_2. Thin film electrodes on platinum substrates were made by evaporating an aqueous solution of $TiOCl_2$ containing appropriate amounts of the following compounds: $Ru(NH_3)_6Cl_3$ in 6M HCl, $(Rh(NO_3)_3$ in 7M HNO_3, $Pd(NO_3)_2$ in 7M HNO_3, $(NH_4)_2IrCl_6$ in 6M HCl and H_2PtCl_6 in 6M HCl.

The photoelectrochemical properties of the thin film electrodes studied are presented in Table 3 and in Figure 4. As shown in Figure 4, very small amounts of Rh, Ru or Pt almost totally quenched the photoresponse. Nevertheless, the action spectra of residual photocurrents in these mixed oxides could be measured using both phase sensitive and dc techniques.

Doped TiO_2 photoelectrodes exhibited poor photoresponses with large dark currents, thus preventing measurements of ΔE_g and V_{fb}. Of the dopants, IrO_2, PdO and Rh_2O_3, rhodium oxide alone extended the wavelength of photoresponse of TiO_2, but in a way analogous to that of Cr_2O_3 in TiO_2 discussed above. The normalized action spectrum of $20TiO_2 \cdot 0.5Rh_2O_3$ is compared to that of TiO_2 in Figure 5. The existence of two distinct band gaps, similar to the Cr_2O_3-TiO_2 system discussed above, may indicate a heterogeneous mixture or the incorporation of Rh_2O_3 into a structure of TiO_2. It is surprising that IrO_2, a metallic conductor, and PdO, ΔE_g = 1.5 eV, did not lower the band gap of TiO_2. Below 5% substitution, the photoresponses were approximately that of pure TiO_2, while increasing concentrations of these dopants did decrease the photoresponse. Iridium oxide and PdO tended to make the V_{fb} somewhat more negative relative to TiO_2 (see Table 3).

E. Platinum-Metal Based Oxide Photoelectrodes: Mixtures of Iron Oxide and Rhodium Oxide

It has been shown that a complete range of solid solutions of Rh_2O_3 in Fe_2O_3 can be obtained (4) while maintaining the corundum structure of αFe_2O_3. This presents the possibility for the isomorphous substitution of iron oxide with rhodium oxide, Rh_2O_3, having not only a smaller band gap than iron oxide but also utilizing 4d electrons. We have, therefore, synthesized a series of compounds $(Fe_{1-x}Rh_x)_2O_3$ with x = 0.5, 0.1, 0.125, 0.25 and 0.5.

Figure 6 shows the integrated photoresponse for a series of iron-rhodium oxide mixtures on a platinum substrate as a function of cutoff wavelength for the filters. Additions of rhodium not only extends the wavelength response for Fe_2O_3 from 600 nm to greater than 830 nm, but the photoresponse at λ >600 nm greatly increases with increasing rhodium content.

The flat band potential (V_{fb}) as well as the band gap for the series of compounds $(Fe_{1-x}Rh_x)_2O_3$ with x = 0, 0.05, 0.1, 0.125, 0.25 and 0.5 is

TABLE 3

PHOTOELECTROCHEMICAL PROPERTIES OF MIXED OXIDE SEMICONDUCTOR PHOTOELECTRODES

Electrode Material	ΔE_g (eV)	V_{fb}	OCP[a] (V)	Photocurrent[b] (mA/cm^2)
$Fe_2O_3 \cdot 0.02TiO_2$[c]	2.00	+0.5	0	1.07
$Fe_2O_3 \cdot 0.02TiO_2 \cdot 0.02RuO_2$[c]	1.95	+0.44	-0.2	1.37
$Fe_2O_3 \cdot 0.02TiO_2 \cdot 0.10RuO_2$[c]	1.96	+0.45	-0.1[d]	1.31
Fe_2O_3	1.98	+0.3	-0.1[d]	1.2
$Fe_2O_3 \cdot 0.02IrO_2$	e	+0.5	+0.2[d]	0.3
$Fe_2O_3 \cdot 0.10IrO_2$	3	+0.3	+0.2	0.43
$Fe_2O_3 \cdot 0.02RuO_2$	1.98	+0.2	-0.2[d]	1.46
TiO_2[c]	3.05	-0.8	-0.7	1.42
$Ti_6Cr_2O_{15}$[c]	2.94(2.05)	-0.57	-0.5[d]	0.97
$Ti_7Cr_2O_{17}$[c]	3.0 (2.05)	-0.4	-0.5[d]	0.76
$Ti_8Cr_2O_{19}$[c]	3.05(2.06)	-0.4	-0.5[d]	0.93
$Ti_9Cr_2O_{21}$[c]	2.96(2.07)	-0.2	-0.4[d]	0.65
$Ti_{12}Cr_2O_{27}$[c]	2.88(2.04)	-0.2	-0.52[d]	1.1
TiO_2	3.05	-0.7	-0.730	1.83
$10TiO_2 \cdot 2.5RuO_2$	e	e	-0.3	0.1
$10TiO_2 \cdot 1RuO_2$	e	e	-0.5	0.15
$10TiO_2 \cdot 0.5RuO_2$	e	e	-0.3	0.28
$20TiO_2 \cdot 2.5Rh_2O_3$	e	e	-0.4	0.093
$20TiO_2 \cdot 1.0Rh_2O_3$	e	e	-0.45	0.1
$20TiO_2 \cdot 0.5Rh_2O_3$	2.7 (1.3)	-0.15	-0.6[d]	0.32
$20TiO_2 \cdot 0.25Rh_2O_3$	2.98(2.0)	0	-0.6[d]	0.24
$20TiO_2 \cdot 0.1Rh_2O_3$	2.94(1.7)	-0.1	-0.8[d]	0.23
$20TiO_2 \cdot 0.25Rh_2O_3 \cdot 0.25Al_2O_3$	2.95(1.6)	-0.1	-0.8[d]	0.13
$10TiO_2 \cdot 2.5PdO$	2.90(2.0)	0	-0.6[d]	0.12
$10TiO_2 \cdot 1PdO$	3.05	-0.35	-0.8[d]	0.77
$10TiO_2 \cdot 0.5PdO$	3.13	-0.25	-0.7[d]	1.4
$10TiO_2 \cdot 2.5IrO_2$	3.17	+0.4	-0.76[d]	0.48
$10TiO_2 \cdot 1CrO_2$	3.0	0	-0.77[d]	0.53
$10TiO_2 \cdot 0.5IrO_2$	3.1	0	-0.8[d]	1.6
$10TiO_2 \cdot 2.5PtO_2$	e	e	-0.3	0.43
$10TiO_2 \cdot 1PtO_2$	e	e	-0.35	0.19
$10TiO_2 \cdot 0.5PtO_2$			-0.75	0.007
$RhNbO_4$	e	e	-0.13	0.08
$9TiO_2 \cdot RhNbO_4$	3.0 (1.9)	-0.35	-0.35	0.51
$RhVO_4$	f	f	-0.1	2.06
$FeCrO_3$	e	e	-0.1	<0.01
$LaCrO_3$	e,f	e,f	0	<0.01
Tl_2O_3	e,f	e,f	+-.15	<0.01

NOTES TO TABLE 3

a. Flat band and open circuit potential versus SCE, pH = 10, 0.25M Na_2SO_4, 0.1M borate buffer.

b. At +1V bias vs. SCE. Illumination was provided by a 150W Xe source. The output was passed through a water filter and defocused to illuminate evenly the electrode surface. The beam was defocused sufficiently to provide approximately 100 mW/cm^2 to the electrode, as measured radiometrically.

c. Sintered polycrystalline pellets. All the rest were thin films on a platinum substrate.

d. These OCP values are a more reliable estimate of the flat band potentials.

e. Difficult to measure due to poor photoresponse, large dark currents, and/or unstable electrode.

f. Difficult to measure due to slow photoresponse.

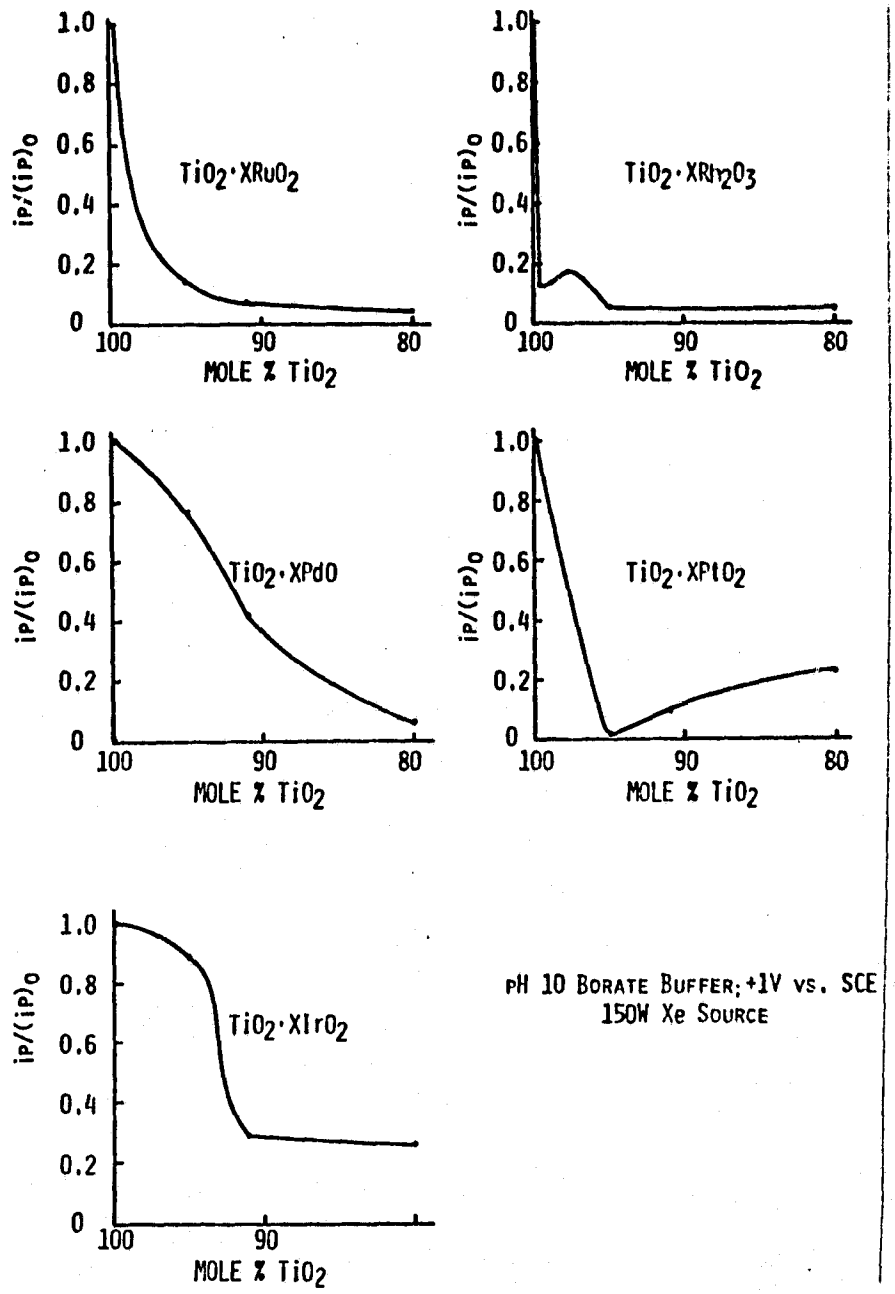

Fig. 4: Effects of added transition metal ions on the photoresponse of thin film TiO_2 electrodes. Photocurrents are recorded at an electrode bias of +1V vs. SCE under the full illumination of a 150W Xe light source. The electrolyte is a borate buffer solution, pH 10.

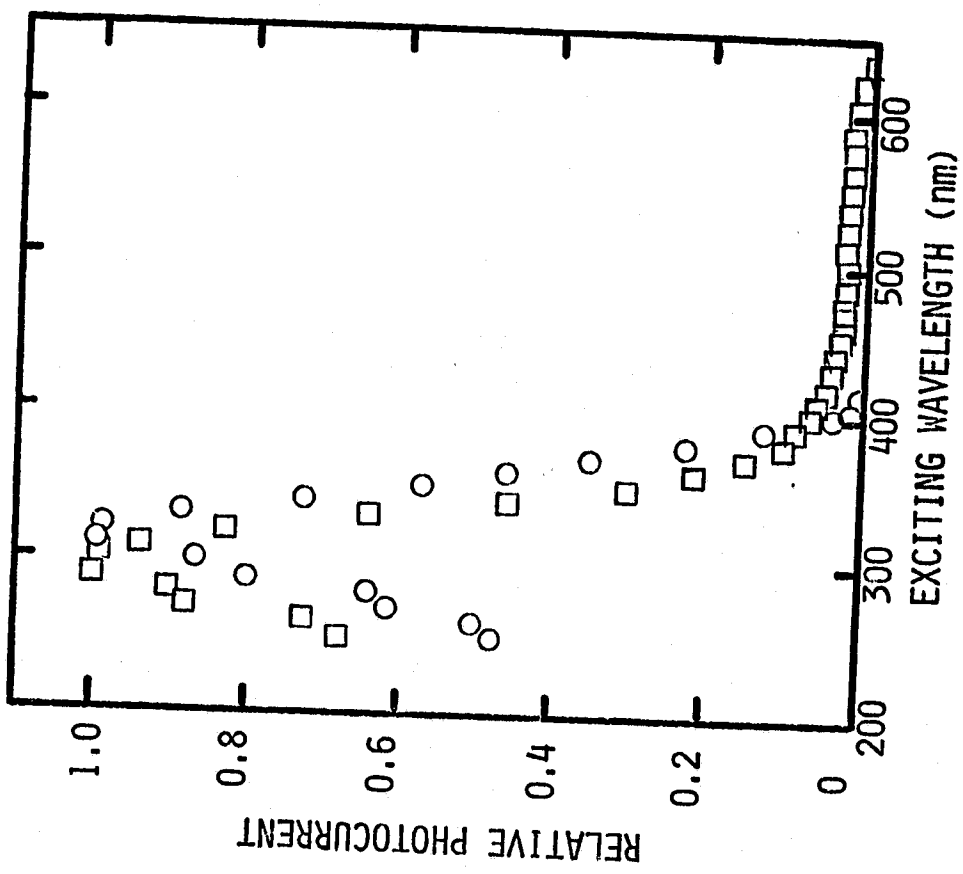

Fig. 5: Action spectra of TiO_2 and rhodium oxide doped TiO_2 thin film electrodes on platinum substrates.

O = TiO_2; □ = $20TiO_2 \cdot 0.5Rh_2O_3$

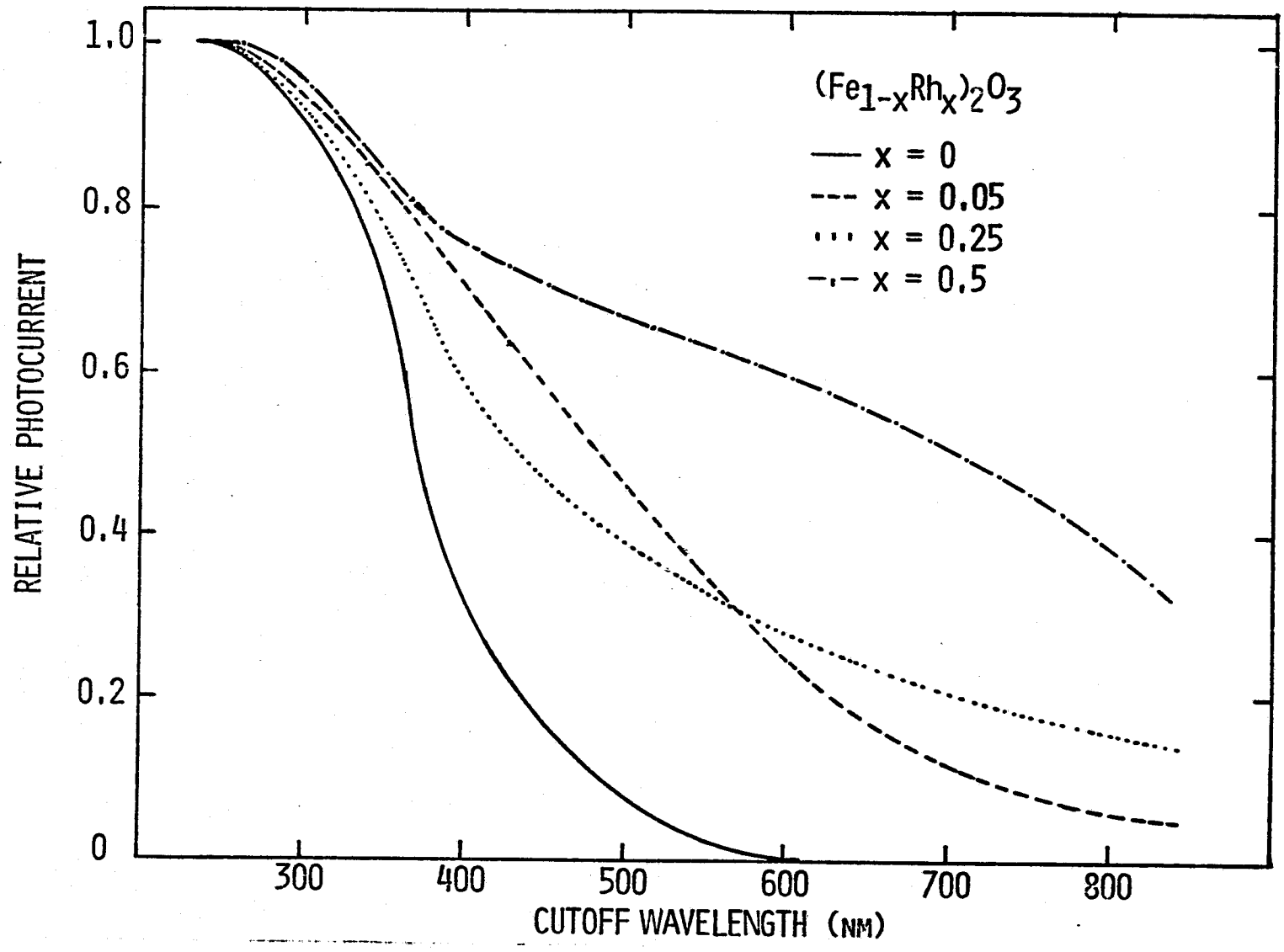

Fig. 6: Integrated photoresponse of mixed, thin film, iron-rhodium oxide photoelectrodes $(Fe_{1-x}Rh_x)_2O_3$ on platinum substrates. All light $>\lambda$ is incident on electrode whereas all light $<\lambda$ is absorbed by filter. Photocurrent at full light was taken as 1.

presented in Table 4. The flat band potential decreases with increasing rhodium substitution. This is to be expected, since the electronegativity of Rh is smaller than that of Fe, 1.45 versus 1.64 on the Allred-Rochow scale (12). Rhodium oxide has rhodium in a low spin d^6 configuration (4) and would be expected to be a small band gap semiconductor analogous to Co^{+3} in $LaCoO_3$ (13). As can be seen in Table 4, the band gap of $(Fe_{1-x}Rh_x)_2O_3$ does decrease from 2 eV at x = 0 to 0.46 eV at x = 0.5.

The same series of compounds $(Fe_{1-x}Rh_x)_2O_3$ with x = 0, 0.05, 0.1, 0.125, 0.25 and 0.5, was also synthesized using Fe_2O_3 (1 atom % TiO_2) as a substrate. The procedures were similar to those used for platinum substrates. The flat band potentials (as determined from the photocurrent onset) and the band gaps (ΔE_g) of these compounds are presented in Table 4. The results correlate very well with those for the platinum substrate, except for x = 0.5 where anomalous behavior is observed. This can be seen in Figure 7, which presents the action spectra of $(Fe_{1-x}Rh_x)_2O_3$ on iron oxide pellets. The visible portion of the response increases with increasing x as expected by the decrease in ΔE_g, except for x = 0.5. This might be due to a changed surface crystal structure caused by prolonged heating. Such effects have been previously observed (4-6).

A more dramatic effect of rhodium is seen when examining the photocurrent produced with polychromatic light at +1V bias versus SCE, as shown in Table 5 and Figure 8. The photocurrent more than doubles upon addition of 5% rhodium and the increase is even further augmented by increasing the pH of the solution. The effect of pH becomes more pronounced with increasing rhodium concentration. The rhodium seems to catalyze water decomposition. Hoare (14) has pointed out that during the electrolysis of water with metal electrodes, the oxygen produced initially reacts with the metal surface to produce surface oxides. Therefore, the potential at which oxygen can start to evolve from the oxide surface is related to the metal/metal oxide couple or, if there is more than one form of oxide, the lower metal oxide/higher metal oxide couple. Rhodium oxide exists in two forms, Rh_2O_3 and RhO_2 (5). The couple Rh_2O_3/RhO_2 has a value of 1.43 volts vs. normal hydrogen electrodes (nhe)(15). Aside from the fact that rhodium enters the band structure of iron oxide as indicated by the lowering of ΔE_g for iron oxide, the catalytic effects of rhodium might be mediated via surface states. An examination of the position of the bands and the redox couples involved (Figure 9) indicates that the overlap of the Rh_2O_3/RhO_2 couple will be greater than that of a hole in the valence band with the OH^-/O_2 couple. The above example is given for $(Fe_{0.75}Rh_{0.25})_2O_3$ with a ΔE_g = 1.54 eV (Table 4). Experiments with quantitative gas collection should give a clearer picture of the actual mechanisms involved.

The current efficiency for the photoelectrochemical production of H_2 and O_2 was also checked for Fe_2O_3 and $(Fe_{0.95}Rh_{0.05})_2O_3$ photoelectrodes. The gases were collected by inverted calibrated pipets having flared ends which were placed above the electrodes. The photocurrent was monitored and it remained constant. The efficiency for hydrogen production was $\approx$100% whereas that for oxygen production was $\approx$85% for both photoelectrodes.

TABLE 4

PHOTOELECTROCHEMICAL PROPERTIES OF THIN FILMS OF IRON OXIDE-RHODIUM OXIDE MIXTURES ON PLATINUM AND IRON OXIDE SUBSTRATES

$(Fe_{1-x}Rh_x)_2O_3$	V_{fb}[a] (volts)		ΔE_g (eV)	
x	Pt	Fe_2O_3[b]	Pt	Fe_2O_3[b]
0	0.5	0.5	2.00	2.00
0.05	0.4	0.4	1.80	1.83
0.1	0.0	0.4	1.70	1.72
0.125	0	0.3	1.60	1.70
0.25		0.3	1.58	1.54
0.5		0.3	0.46	1.42

[a] pH = 10 vs. SCE.
[b] Sintered pellets doped with 1 atom % TiO_2.

TABLE 5

PHOTORESPONSE OF IRON OXIDE-RHODIUM OXIDE MIXTURES ON IRON OXIDE SUBSTRATES[a]

$(Fe_{1-x}Rh_x)_2O_3$	pH			
x	10		13	
	Photocurrent[b,c] (mA/cm^2)	Dark Current[b] (mA/cm^2)	Photocurrent[b,c] (mA/cm^2)	Dark Current[b] (mA/cm^2)
0	1.07	-	1.64	-
0.05	2.69	-	4.64	-
0.1	1.66	0.03	4.29	1.36
0.125	2.06	0.06	5.00	1.40
0.25	2.29	0.17	9.71	4.57
0.5	2.34	0.23	19.14	15.7

[a] Substrates were sintered pellets of Fe_2O_3 doped with 1 atom % TiO_2.
[b] At +1V bias versus SCE.
[c] Polychromatic light.

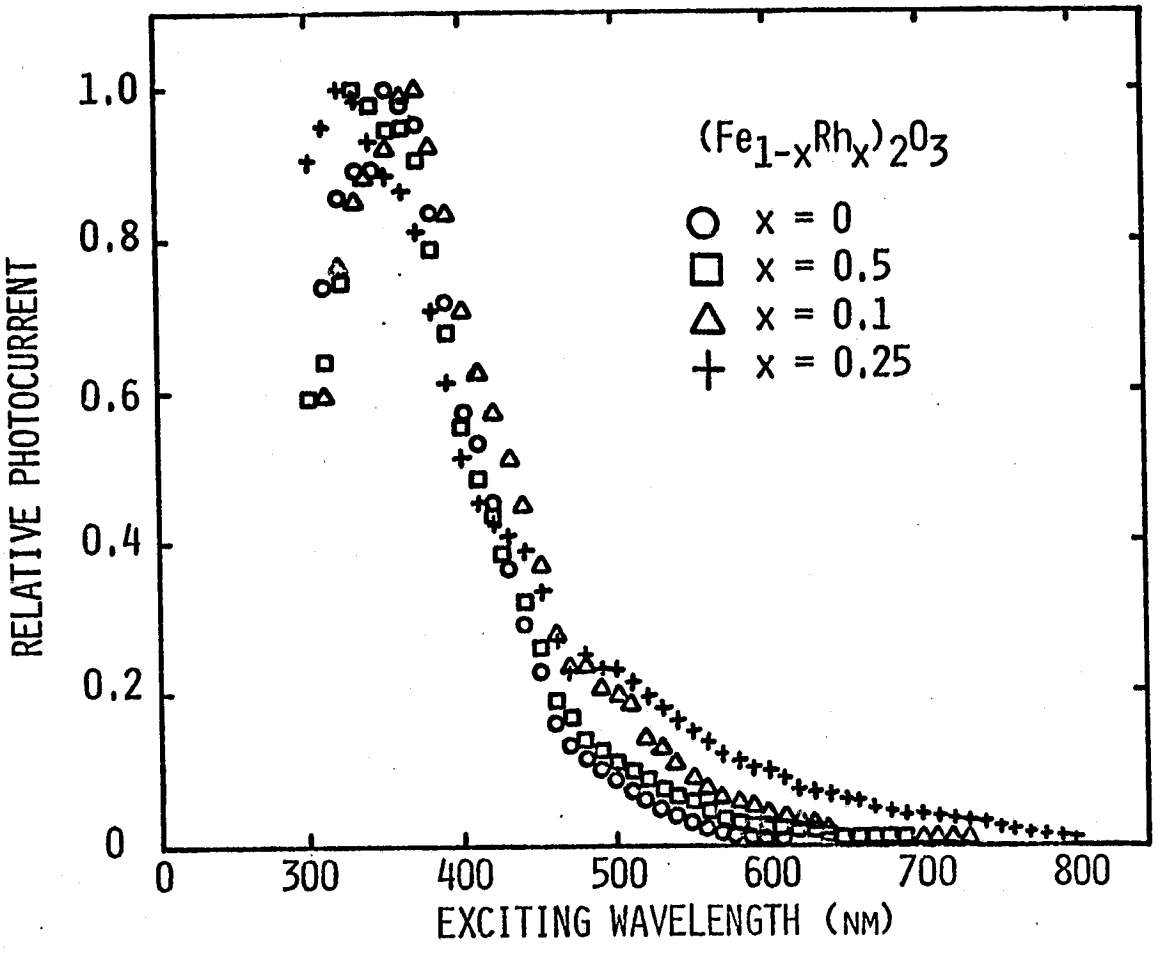

Fig. 7: Action spectra of Fe_2O_3 and Rh_2O_3 doped Fe_2O_3 thin film electrodes on sintered polycrystalline $Fe_2O_3 \cdot 0.02TiO_2$ substrates.

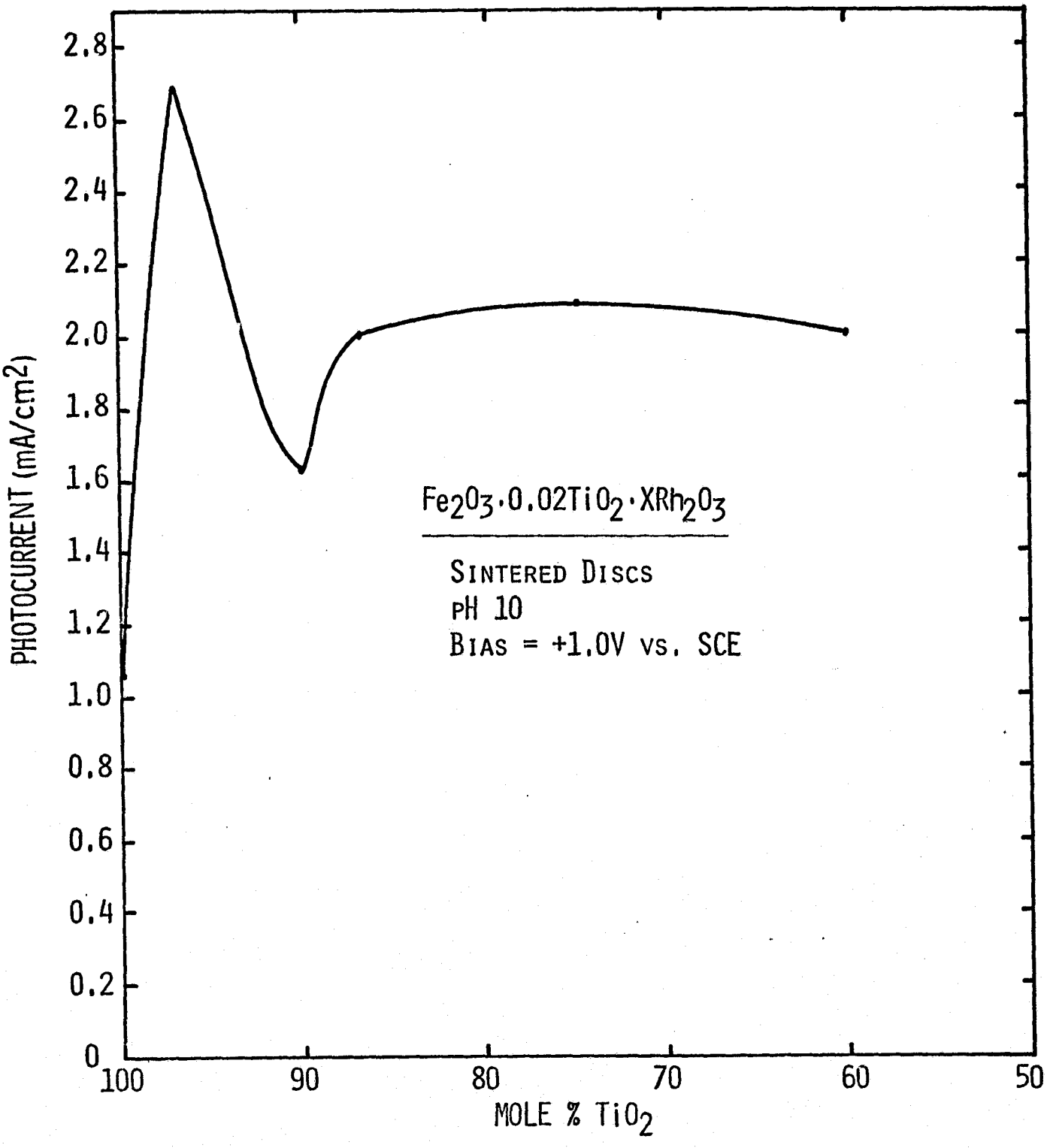

Fig. 8: Effects of added Rh_2O_3 on the anodic photocurrent of Fe_2O_3 sintered disc electrodes.

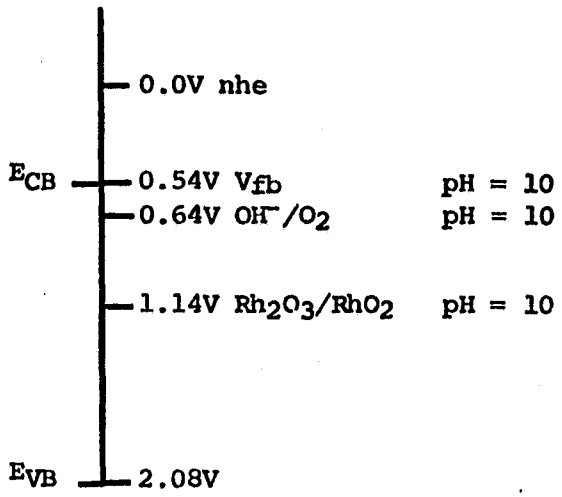

Fig. 9: Relative positions of redox and band energies in $Fe_2O_3 \cdot xRh_2O_3$/pH 10 aqueous electrolyte junction.

We have also evaluated our methods for the measurements of flat band potentials (V_{fb}). We have been using the open circuit potential (OCP) as an estimate of V_{fb} and also that derived from the Schottky barrier model of the semiconductor-electrolyte interface, the intercept of a plot of (photocurrent)^2 vs. bias voltage giving V_{fb}. We have now also estimated V_{fb} from the instantaneous photovoltage developed as a function of bias voltage. Typically, the instantaneous photovoltage developed with a chopped light beam is measured as a function of bias voltage. V_{fb} is the point where the photovoltage becomes zero or changes sign. This method, as well as the OCP, gives estimates of V_{fb} consistent with literature values, whereas the Schottky barrier model gives V_{fb}s which are sometimes spurious. A typical example is Fe_2O_3, at pH 10, the V_{fb} given versus SCE: literature value, V_{fb} = -0.15V; OCP, V_{fb} = 0.0V; instantaneous photovoltage, V_{fb} = -0.3V; Schottky barrier model, V_{fb} +0.5V.

Attempts were also made to grow single crystals of Fe_2O_3 and rhodium substituted Fe_2O_3 by vapor transport. Rhodium oxide hydrate was converted to the corundum oxide by heating in air for 2 days at 700°C. A charge consisting of ≈1g of mixed Fe_2O_3-Rh_2O_3 and ≈20 mg of tellurium was sealed in a 15-20 cm quartz tube, 15 mm in diameter, containing ≈380 mm (Hg) of Cl_2 gas. The tube was heated in a back transport mode (900°C/450°C) for 24 hours and then in the transport mode (900°C/1000°C) for 5 days. Only very small crystallites were produced. Apparently there was insufficient Cl_2 in the quartz tube for adequate crystal growth, which may have been induced by a fault in the pressure measuring system.

F. Other Mixed Oxides of Fe_2O_3 Parentage

Similar to the rhodium doped Fe_2O_3 photoelectrodes reported above, we have incorporated RuO_2 and IrO_2 into Fe_2O_3 polycrystalline pellets and thin films. The pellets containing RuO_2 were made by our standard double sinter technique, final sinter being at 1250°C for 20 hours. Thin films were made on platinum substrates by evaporation of aqueous $Fe(NO_3)_3$ solutions containing $Rh(NH_3)_6Cl_3$ or $(NH_4)_2IrCl_6$. Photoelectrochemical characteristics of these electrodes are presented in Table 6 and Figure 10. The action spectra of iron oxide and ruthenium doped iron oxide photoelectrodes are presented in Figure 11. There appears to be little effect of ruthenium on the action spectra. The presence of ruthenium also did not affect the V_{fb} and ΔE_g although, as shown graphically in Figure 9, it did increase the photoresponse slightly. Since RuO_2 has metallic conductivity, these results imply that RuO_2 is insoluble in Fe_2O_3. This was confirmed by an X-ray powder diagram. The addition of IrO_2 to Fe_2O_3 tends to decrease the photocurrent and increase the dark current to the levels of the photocurrent. The large dark currents as well as the apparent slow photoresponse precluded the measurement of ΔE_g and V_{fb}, although addition of IrO_2 made the open circuit potential of Fe_2O_3 more negative (see Table 6).

TABLE 6

PHOTOELECTROCHEMICAL PROPERTIES OF MIXED IRON-OXIDE PLATINUM METAL OXIDE PHOTOELECTRODES

Electrode Material	ΔE_g (eV)	V_{fb}[a]	Photocurrent[b] (mA/cm^2)
$Fe_2O_3 \cdot 0.02TiO_2$[c]	2.00	0	1.07
$Fe_2O_3 \cdot 0.02TiO_2 \cdot 0.02RuO_2$[c]	1.95	-0.2	1.37
$Fe_2O_3 \cdot 0.02TiO_2 \cdot 0.10RuO_2$[c]	1.96	-0.1	1.31
$Fe_2O_3 \cdot 0.02RuO_2$	1.98	-0.2	1.46
Fe_2O_3	1.98	-0.1	1.2
$Fe_2O_3 \cdot 0.02IrO_2$	d	+0.2	0.3
$Fe_2O_3 \cdot 0.10IrO_2$	3.0	+0.2	0.43

[a] Flat band and open circuit potential versus SCE, pH = 10, 0.25M Na_2SO_4, 0.1M borate buffer.

[b] At +1V bias vs. SCE.

[c] Sintered polycrystalline pellets. All the rest were thin films on a platinum substrate.

[d] Difficult to measure due to poor photoresponse, large dark currents, and/or unstable electrode.

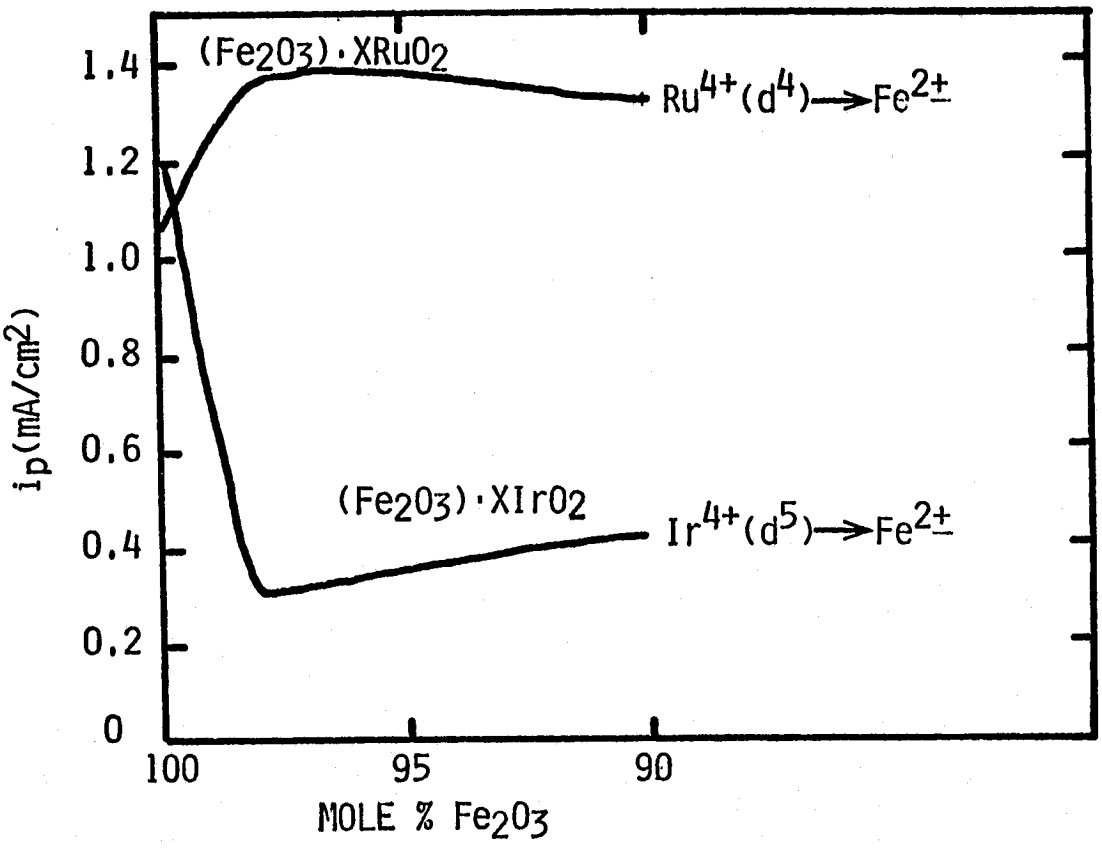

Fig. 10: Photoresponse of $Fe_2O_3 \cdot xMO_2$ thin film electrodes under 150W Xe source illumination.

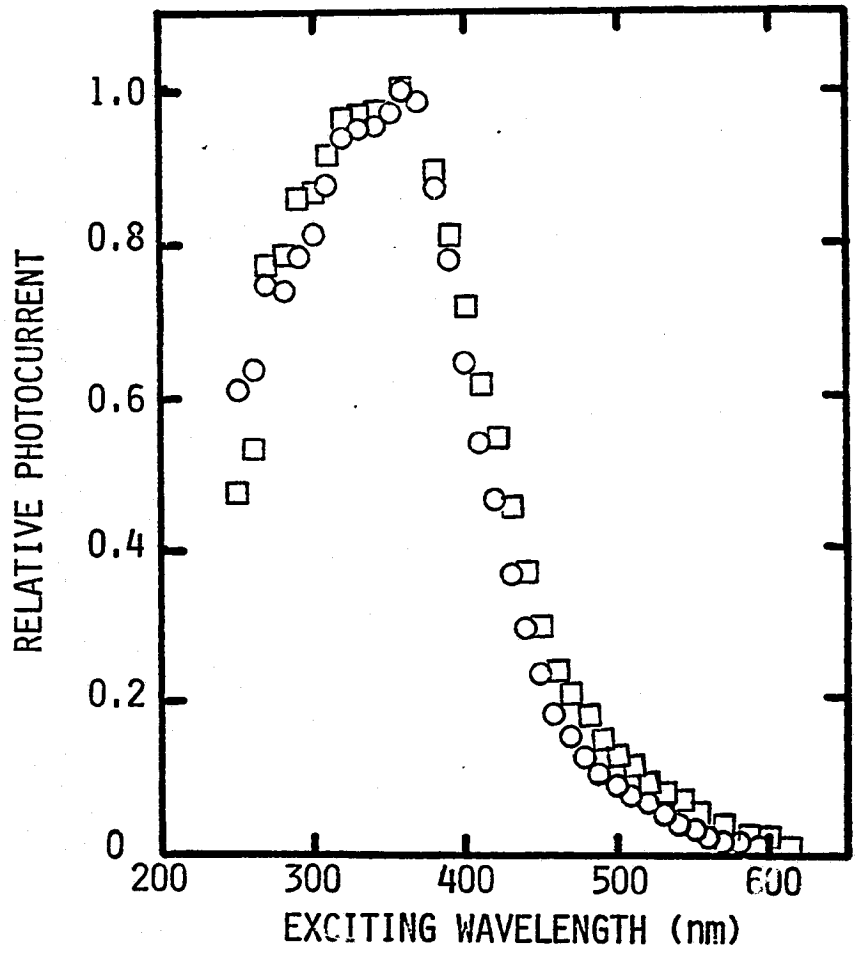

Fig. 11: Action spectra of Fe_2O_3 and RuO_2 doped Fe_2O_3 sintered polycrystalline electrodes.

O = $Fe_2O_3 \cdot 0.02TiO_2$; □ = $Fe_2O_3 \cdot 0.02TiO_2 \cdot 0.02RuO_2$

G. Photoelectrochemical Effects of Carbonate and/or Bicarbonate Ions

Originally we had added carbonate and bicarbonate ions to the electrolyte in order to suppress the large dark currents produced by $MgTiFe_2O_6$ photoelectrodes (1). One observed result was an increase in the photocurrent. We have performed these experiments with iron oxide photoelectrodes and the results for two separate pellets are shown in Figure 12. The presence of $CO_3^=/HCO_3^-$ increased the photocurrent by factors of 1.29 and 1.66 relative to the photoresponse in the absence of $CO_3^=/HCO_3^-$. Only the relative photoresponse is significant, since the absolute photoresponse of iron oxide tends to vary from pellet to pellet. Two other experiments indicated increases by factors of 1.2 and 1.16. Photocurrents were stable over a period of about an hour both in the presence and absence of HCO_3^- and $CO_3^=$. Since $CO_3^=$ and HCO_3^- exist in a pH dependent equilibrium, we tested the photoresponse as a function of pH and $CO_3^= + HCO_3^-$ concentration (Table 7). At pH $\approx$8.5, HCO_3^- predominates; at pH = 10, both species $HCO_3^- + CO_3^=$ are present; and at pH = 13, only $CO_3^=$ is present. Although there is quite a scatter of data, it can be seen from Table 7 that HCO_3^- appears to be the photoelectrochemically active ion. The same results were found from chromium and aluminum doped TiO_2 (T-45, Table 7), although again the data were scattered. An attempt was made to create specific adsorption sites in Fe_2O_3 by Al_2O_3 doping. The results for F-24 and F-25 (Table 7) follow the general pattern of increasing photocurrent with increasing HCO_3^- concentration.

The effects of pH, HCO_3^- and $CO_3^=$ concentration on the flat band potential are shown for Fe_2O_3, F-24 and T-45 in Table 8. The flat band potential varies with pH as expected; surprisingly, it is independent of HCO_3^- or $CO_3^=$. If HCO_3^- had specific adsorption sites on these photoelectrodes, then the V_{fb} should change with HCO_3^- at a given pH. $HCO_3^- + CO_3^=$ had no effect on the photoelectrochemical properties of $BaTiO_3$, $SrTiO_3$ and TiO_2 photoelectrodes. It is possible that $HCO_3^- + CO_3^=$ has equivalent effects on all the electrodes studied except that water is already very efficiently oxidized at the $BaTiO_3$, $SrTiO_3$ and TiO_2 surface and therefore no improvement is seen. However, water oxidation at the iron oxide and chromium aluminum doped titanium dioxide surfaces must be less efficient and, therefore, the effects of bicarbonate are discernible.

The effects of $HCO_3^- + CO_3^=$ additions on the photoresponse of rhodium doped iron oxide photoelectrodes were also investigated and are summarized in Table 9. Addition of 1M $[HCO_3^- + CO_3^=]$ results in a significant increase of the photoresponse. At 12.5% rhodium substitution, the increase in photocurrent is already maximum and is approximately twice as large as that in the absence of $HCO_3^-/CO_3^=$. At higher rhodium substitution, the dark current increase more rapidly in the presence of $HCO_3^-/CO_3^=$ (see Table 9). It would appear that rhodium is creating specific electrochemically active adsorption sites for bicarbonate ions. We had previously

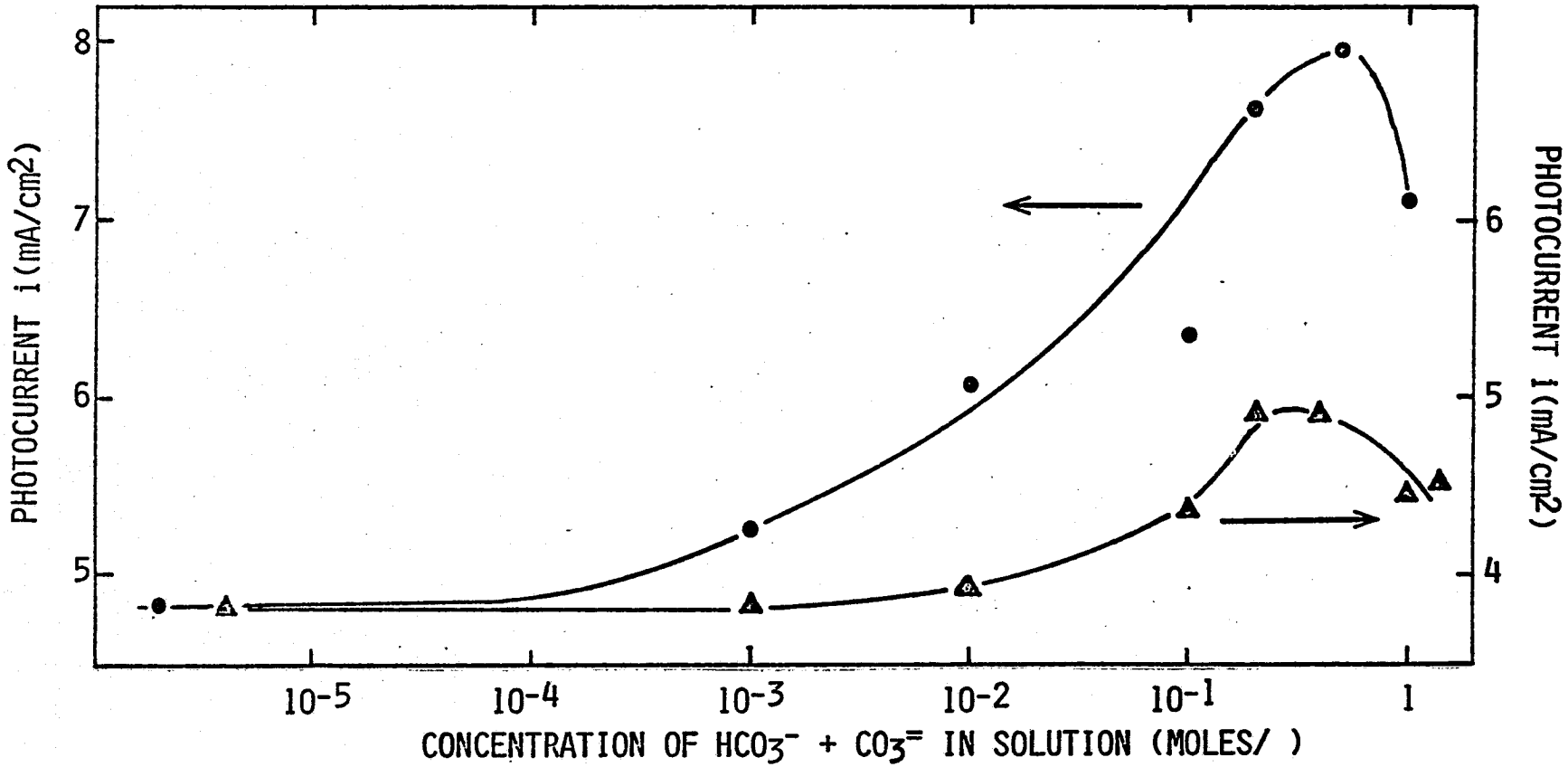

Fig. 12: Effect of bicarbonate/carbonate ions on the photoresponse of the Fe_2O_3 (1% TiO_2) photoelectrodes. ● and ▲ represent two different photoelectrodes. All solutions contained 0.25M Na_2SO_4 and 0.1M borate buffer and are adjusted to final pH = 10. First points on the left of the curves are photoresponses at $[HCO_3^- + CO_3^=] = 0$.

TABLE 7

PHOTOELECTROCHEMICAL EFFECTS OF BICARBONATE AND CARBONATE IONS

Photoelectrode Composition (Code)	Photocurrent[a] (mA/cm^2)	pH[b]	$[HCO_3^- + CO_3^=]$[c] (moles/liter)
$Fe_2O_3 \cdot 0.02TiO_2$	0.89	8.5	none
	2.04	8.5	1 (HCO_3^- only present)
	5.0	8.5	none
	5.1	8.5	1 (HCO_3^- only present)
	3.7	13	none
	3.7	13	1 ($CO_3^=$ only present)
	6.0	13	none
	4.1	13	1 ($CO_3^=$ only present)
$Fe_2O_3 \cdot 0.11Al_2O_3 \cdot 0.022TiO_2$ (F-24)	0.92	10	none
	0.93	10	1
	0.37	8	none
	0.55	8	1 (HCO_3^- only present)
$Fe_2O_3 \cdot 0.25Al_2O_3 \cdot 0.05TiO_2$ (F-25)	0.91	10	none
	0.99	10	1
	0.44	8	none
	0.47	8	1 (HCO_3^- only present)
$Ti_{14}Cr_2O_{31} \cdot 0.1Al_2O_3$ (T-45)	0.72	10	none
	0.72	10	1
	1.22	10	1
	0.83	8.5	none
	1.4	9	1

[a] Measured at a bias of +1 volt vs. SCE.

[b] Solutions at pH 8-10 contained borate buffer + 0.25M Na_2SO_4; pH 13 contained only KOH.

[c] Added as Na HCO_3 and Na_2CO_3.

TABLE 8

EFFECT OF pH AND BICARBONATE AND CARBONATE IONS ON THE FLAT BAND POTENTIAL OF SOME METAL OXIDES

Photoelectrode Composition (Code)	$[HCO_3^- + CO_3^=]$[a] (moles/liter)	Flat Band Potential V_{fb}, Volts vs SCE[b]		
		pH = 8.3[c]	pH = 10[c]	pH = 13[d]
$Fe_2O_3 \cdot 0.02TiO_2$	0	0.4	0.34	0.1
	10^{-4}	0.39	-	-
	10^{-2}	0.42	-	-
	10^{-1}	0.45	0.35	0.05
	1	0.43	0.32	0.05
	2	0.37	-	-
$Fe_2O_3 \cdot 0.11Al_2O_3 \cdot 0.022TiO_2$ (F-24)	0	0.48	0.3	0.05
	10^{-4}	0.5	-	-
	10^{-2}	0.48	-	-
	10^{-1}	0.39	0.35	0.0
	1	0.48	0.27	0.0
	2	0.40	-	-
$Ti_{14}Cr_2O_3 \cdot 0.1Al_2O_3$ (T-45)	0	-0.39	-0.4	-0.67
	10^{-4}	-0.36	-	-
	10^{-2}	-0.36	-	-
	10^{-1}	-0.36	-0.45	-0.67
	1	-0.38	-0.43	-0.7
	2	-0.41	-	-

[a] Added as $NaHCO_3$ and Na_2CO_3.
[b] V_{fb} measured from a plot of (photocurrent)^2 vs. bias potential using monochromatic illumination.
[c] Contained borate buffer + 0.25M Na_2SO_4.
[d] Adjusted with KOH.

TABLE 9

EFFECT OF BICARBONATE/CARBONATE IONS ON THE PHOTORESPONSE OF MIXED IRON OXIDE-RHODIUM OXIDE PHOTOELECTRODES[a]

$(Fe_{1-x}Rh_x)_2O_3$ x	Photocurrent[b] (mA/cm²) With[c] $HCO_3^- + CO_3^=$	Photocurrent[b] (mA/cm²) Without $HCO_3^- + CO_3^=$	Dark Current (mA/cm²) With[c] $HCO_3^- + CO_3^=$	Dark Current (mA/cm²) Without $HCO_3^- + CO_3^=$
0	1.09	1.27	-	-
0.05	2.0	2.69	-	-
0.1	3.2	1.66	0.04	0.03
0.125	4.3	2.06	0.1	0.06
0.25	4.3	2.29	0.47	0.17
0.5	4.3	2.34	1.9	0.23

[a] Substrates were sintered pellets of Fe_2O_3 doped with 1 atom % TiO_2.
[b] pH = 10, at +1V bias versus SCE, polychromatic light.
[c] $[HCO_3^- + CO_3^=]$ = 1 molar.

attempted to create just such sites by substituting aluminum oxide in iron oxide with only marginal success. The increased selective oxidation of bicarbonate would result in the catalyzed photooxidation of water via the following mechanisms:

I.

$$2CO_3^= \rightarrow 2\cdot CO_3^- + 2e^-$$
$$2\cdot CO_3^- + 2H_2O \rightarrow H_2O_2 + 2OH^- + 2CO_3$$
$$H_2O_2 \rightarrow H_2O + \tfrac{1}{2}O_2$$
$$2CO_2 + 4OH^- \rightarrow 2H_2O + 2CO_3^=$$

Net: $2OH^- \rightarrow H_2O + \frac{1}{2}O_2 + 2e^-$

II.

$$2CO_3^= \rightarrow 2{:}CO_3 + 4e^-$$
$$2{:}CO_3 \rightarrow 2CO_2 + O_2$$
$$2CO_2 + 4OH^- \rightarrow 2H_2O + 2CO_3^=$$

Net: $4OH^- \rightarrow 2H_2O + O_2 + 4e^-$

Another interesting aspect of the $CO_3^=$ oxidation is the possibility of precluding peroxide formation at Fe_2O_3. In Figure 13, a diagram of the Fe_2O_3 band energetics is shown, with the various electrochemical potentials important in this system. The CO_3^-/CO_3^{2-} potential determined by Grätzel (16) is at ~1.5V vs. SCE at alkaline pHs. This reaction is therefore easier than H_2O_2 formation via a free radical mechanism. In TiO_2 mediated photoelectrolysis, ·OH radicals have been detected on the surface which can act as carrier recombination centers (17).

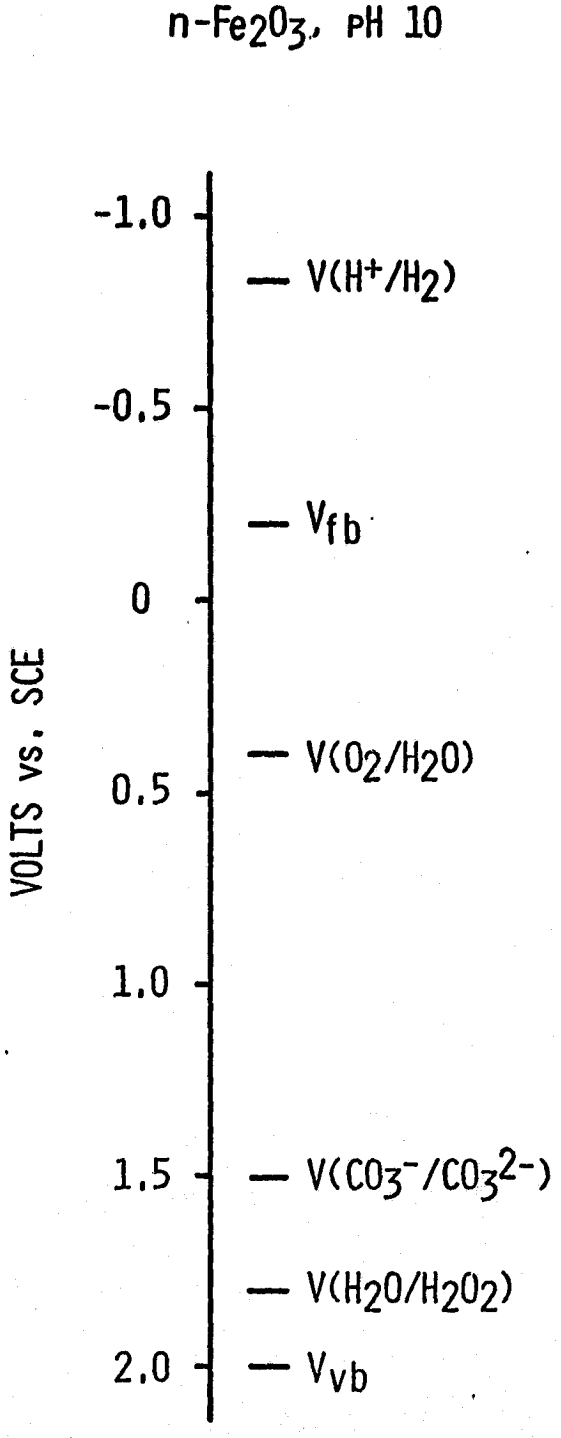

Fig. 13: Interfacial energetics of Fe_2O_3 conduction and valence bands at pH 10, along with relevant solution redox potentials.

H. Other Mixed Oxide Photoelectrodes

The compounds $FeCrO_2$ (corundum), $LaCrO_3$ (perovskite), and Tl_2O_3 were prepared as thin films on platinum substrates by evaporation of solutions containing a 0.1M mixture of the respective nitrates. $RhNbO_4$ (rutile) and $9Ti_2O_4$ $RhNbO_4$ were prepared by evaporation of solutions of $NbCl_5$, $Rh(NO_3)_3$ and $TiOCl_3$ in concentrated HCl. $RhVO_4$ (rutile) was prepared by evaporation of a solution containing $Rh(NO_3)_3$ and NH_4VO_3.

The photoelectrochemical properties of these compounds are presented in Table 1. $FeCrO_3$ was unstable whereas $LaCrO_3$ and Tl_2O_3 and slow photoresponses with large dark currents. The composition of the Tl_2O_3 electrode is questionable, since it has a low decomposition temperature of $\approx$200°C. $RhNbO_4$ had a weak and slow photoresponse. Its addition of TiO_2 resulted in more positive V_{fb}, decreased photoresponse and two band gaps of 3 and 1.0 eV, similar to the Cr_2O_3-TiO_2 discussed above. $RhVO_4$ developed a large photocurrent, yet its large dark current and slow photoresponse precluded further characterization. This compound is the first reported photoelectrode utilizing vanadium. It has a stable photocurrent during a 15 minute test with no visible alteration of its surface.

An iron-nickel compound of perovskite structure has been prepared (Table 1). It was an n-type semiconductor and was unstable to dissolution under illumination. The mixed oxide photoelectrodes of spinel structure that were synthesized are presented in Table 1. All were n-type semiconductors. Both L-5 and L-7 gave slow photoresponses. Photocurrents under full illumination from the 100 watt Xe lamp at +1V bias vs. SCE were 0.9 mA/cm^2 for L-5 and 0.09 mA/cm^2 for L-7, although the magnitudes of the dark currents were equivalent to the photocurrents. Both had photocurrent onsets of $\geq$0 volts vs. SCE, the onset being an approximation of the flat band potential (V_{fb}). The spinel oxides, S-3, S-4 and S-5, gave photocurrents of only $\approx$0.1 mA/cm^2 under full illumination at +1V bias vs. SCE. Photocurrent onsets occurred at positive bias voltages. The above mentioned spinel oxide photoelectrodes are considered to be marginal at best and no further investigations will be carried out with them.

A new n-type photoelectrode, the spinel $CdIn_2O_4$ (18), has been synthesized as a thin film on a platinum substrate. Both Cd^{+2} and In^{+3} are $4d^{10}$ ions. This electrode develops 1.1 mA/cm^2 of photocurrent under full illumination at +1V bias vs. SCE in pH = 10 buffer. The band gap is an indirect one (see discussion in A.3) and has a value of 2.33 eV. The flat band potential is -0.4V at pH = 10 and -0.6V at pH = 13. This is the expected result if OH^- (H^+) binding occurs with a concurrent change in potential of 0.059/pH unit. The action spectrum for photocurrent is shown in Figure 14. It favors higher energy light, indicating a low diffusion length for holes in the films.

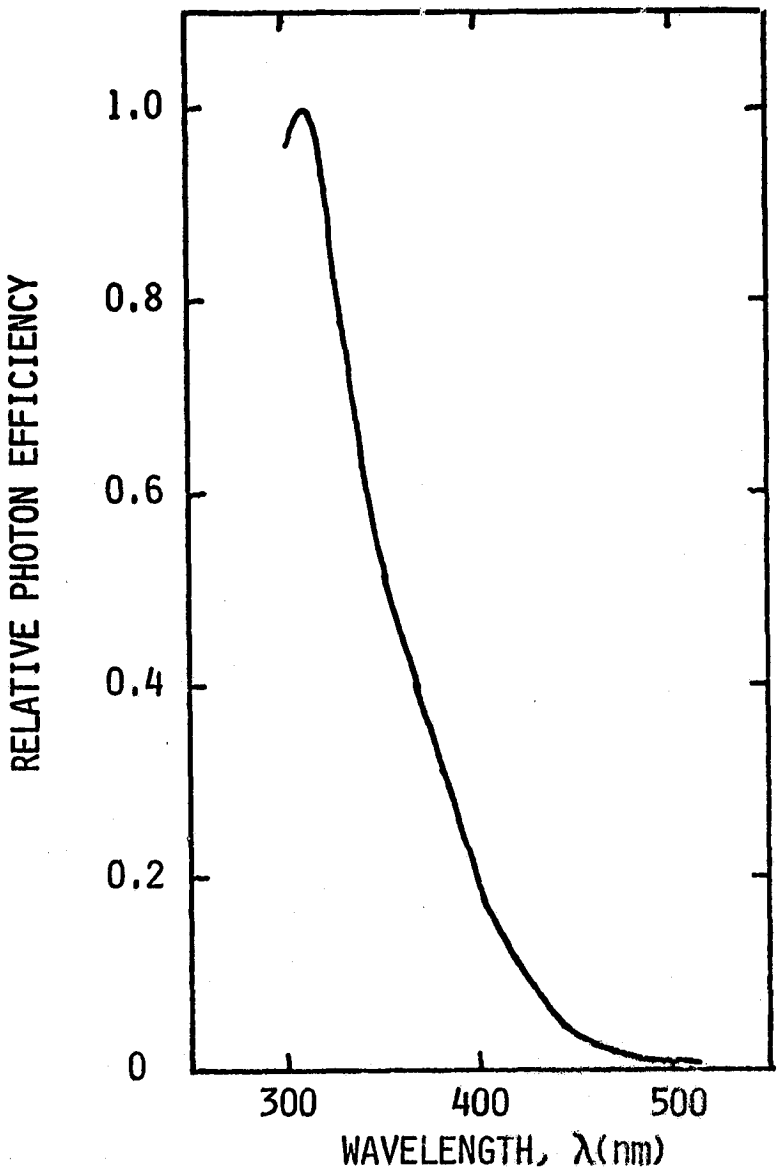

Fig. 14: Photoresponse of thin $CdIn_2O_4$ films on platinum substrate. Bias was +1V versus SCE. Solution was buffered at pH = 10 with borate buffer and contained 0.25M Na_2SO_4.

III. PHOTOELECTROCHEMICAL DIODES

A. Particulate Semiconductor Configuration

During the past year, work was initiated on systems which might be employed for practical photoelectrolytic solar energy conversion. A very promising configuration is that in which the photoelectrochemical reaction occurs on individual semiconductor particles suspended in solution. A Schottky-type particle is illustrated in Figure 15. Here, a metal is deposited on a semiconductor. Under irradiation, each particle can act as a tiny electrochemical cell. If the semiconductor is n-type, the anodic half-reaction will occur on its surface, and the cathodic half-reaction will occur on the metal.

In order to decompose water on such a particle, the semiconductor must be a "Class I" material (2), i.e., with E_c and E_v straddling the H_2 and O_2 evolution potentials. The best example of a stable Class I photoanode found to date is $SrTiO_3$. Bard (19) and Wrighton (20) have already observed H_2O decomposition on partially platinized $SrTiO_3$.

We conducted some exploratory work on photoelectrolysis using partially platinized semiconductor particles. Both platinization and water photoelectrolysis were conducted in the apparatus shown in Figure 16. Two methods of platinization have been used: photodeposition and thermal decomposition of platinic acid-semiconductor slurries. The photodeposition method as published (19) yielded poor results. The semiconductor powders were not significantly darkened (as had been reported) and the sample of $SrTiO_3$/Pt thus prepared displayed low gas evolution under irradiation. Further heating of the photodeposition product (300°C overnight) proved to blacken the powder and improve the photochemical gas yield (presumably H_2/O_2). The post-deposition heating was incorporated into the procedure for all other samples.

The thermal decomposition method gave a much darker and heavier Pt deposit, but the amount of platinum actually plated onto the semiconductor (rather than in small agglomerates) is questionable. While this method worked for $SrTiO_3$, it did not work for $MoSe_2$, WSe_2, Fe_2O_3, or CdS (Table 10).

Results of photoelectrolysis of water using the platinized $SrTiO_3$ particles are summarized in Table 11. Except as noted, all photolyses were conducted at 32°C with 0.5M NaOH electrolyte. The process seems to have an induction time of $\sim$600 sec. This may be due to the evolved gas dissolving in the electrolyte and reaching saturation in $\sim$600 sec.

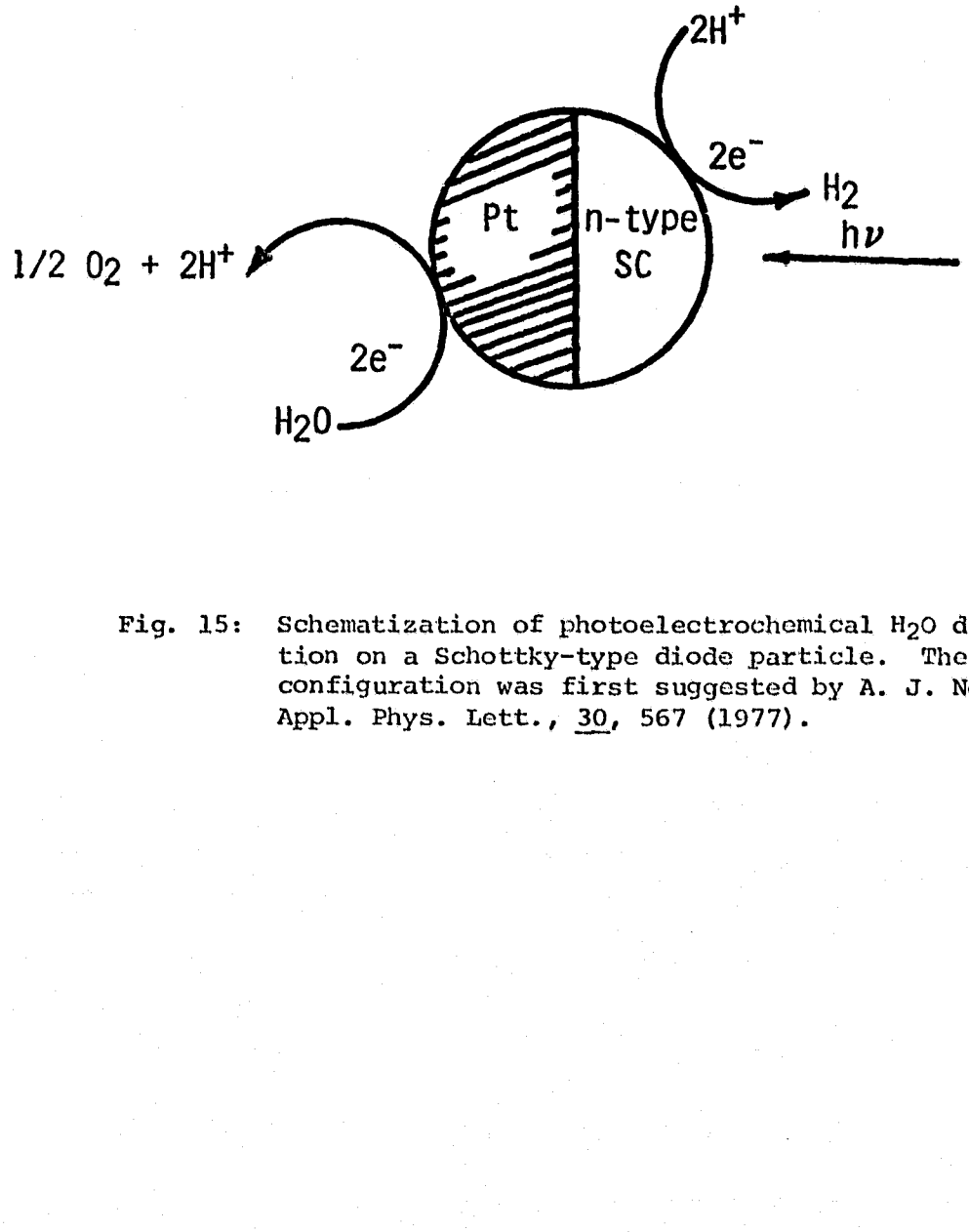

Fig. 15: Schematization of photoelectrochemical H_2O decomposition on a Schottky-type diode particle. The diode configuration was first suggested by A. J. Nozik, Appl. Phys. Lett., 30, 567 (1977).

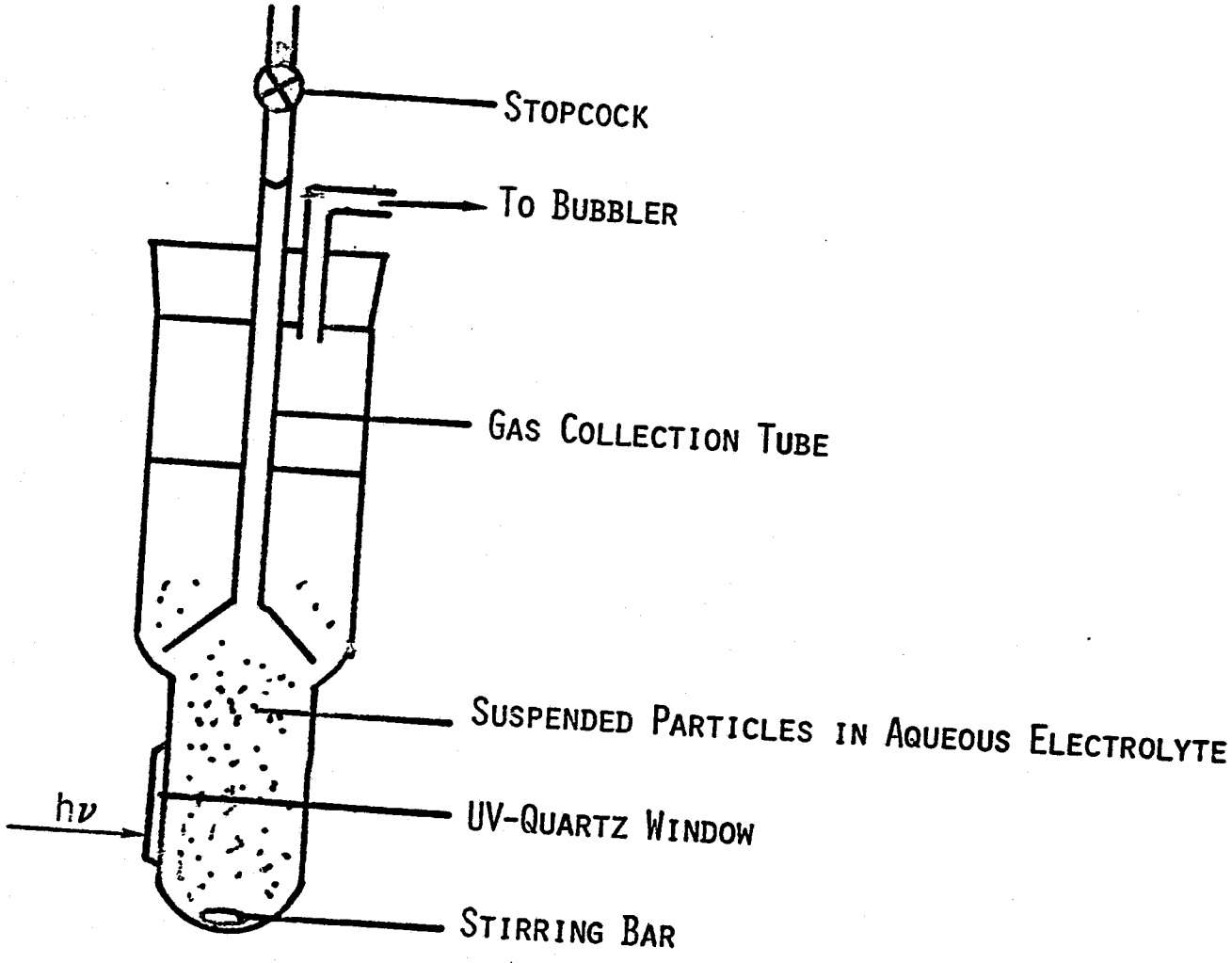

Fig. 16: Cell for monitoring photoelectrochemical gas evolution on semiconductor diode particles.

TABLE 10

SUMMARY OF PLATINIZATION OF SEMICONDUCTORS

PD = Photodecomposition
TD = Thermal Decomposition

Sample No.	Compound	Method	Results	Comments
1	$SrTiO_3$	TD	good	1.55×10^{-2} mg Pt/mg $SrTiO_3$ by AAS, good gas evolution
2*	$SrTiO_3$	PD	poor	1.33×10^{-3} mg Pt/mg $SrTiO_3$ by AAS, room temperature
4*	$SrTiO_3$	PD	poor	4.70×10^{-1} mg Pt/mg $SrTiO_3$ by AAS, 43°C
4A	$SrTiO_3$	PD	good	post-deposition heated
5	$SrTiO_3$	PD	poor	attempted photodeposition using "plat-grade"concentrate as platinizing agent
5A	$SrTiO_3$	PD	poor	" " " "
6	$MoSe_2$	TD	poor	no gas evolution under irradiation with or without 1M LiI electrolyte
7	WSe_2	TD	poor	" " " "
8	$BaTiO_3$	TD	poor	no darkening
9	CdS	TD	failure	decomposed most of sample; remainder gave no gas
-	Fe_2O_3	TD	failure	no gas evolution under irradiation with or without LiI
10	$SrTiO_3$	PD	good	--
11	CdS	PD	good	--

*Not post-deposition heated.

TABLE 11

PHOTOELECTROLYSIS OF H_2O USING
Pt-$SrTiO_3$ PARTICLES

Sample No.	Method of Preparation	Rate of Gas Evolution	Comments
1	TD	0.16 ml/1120 sec = 1.4×10^{-4}	--
4	PD	0.01/6000 = 1.7×10^{-6}	Fatigued
4	PD	0.08/5500 = 1.5×10^{-5}	Fatigued
4	PD	0.06/1900 = 3.2×10^{-5}	Particle size too small, loading too high; fatigued
5	PD	ϕ	--
10	PD	0.04/4500 = 8.9×10^{-6}	Fatigued
10	PD	0/3000 = 0	6M NaOH electrolyte

The fatigue problem seems the most serious. This problem had been reported by Wrighton (20) using the conventional single crystal and Pt counter electrode configuration. He attributed the problem to deplatinization, and found that a "fatigued" crystal could be "revived" by replatinization. The need for additional investigation of the nature and amount of Pt deposits formed on the semiconductor powders is indicated.

B. CdS Photoelectrochemical Diodes

Some preliminary investigations have been carried out on the fabrication of H_2-producing photoelectrochemical diodes which employ an "easier" oxidation than O_2 evolution. We have chosen initially to investigate the CdS/Pt diode in a basic electrolyte containing 1M Na_2S and 1M NaOH. As shown in Figure 17, the resulting photoelectrochemical reaction is the oxidation of S^{-2} (to polysulfide) by holes on the CdS and the reduction of H^+ (or H_2O) by electrons on the Pt. The S^{2-} is necessary to suppress CdS photodissolution.

In order to achieve efficient photoelectrolysis on the unbiased diode, resistivity between the crystal and metal must be minimized. Our first attempts to attach a Pt metal electrode to a CdS crystal using Ag epoxy failed to produce an active diode, probably due to the non-ohmicity of the semiconductor-metal contact.

Diodes were successfuly prepared from n-CdS single crystals as follows: A square crystal of n-CdS (3 mm x 3 mm x 1 mm, ρ = 1Ω-cm) was obtained from Cleveland Crystals. The surface was first etched for 30 sec

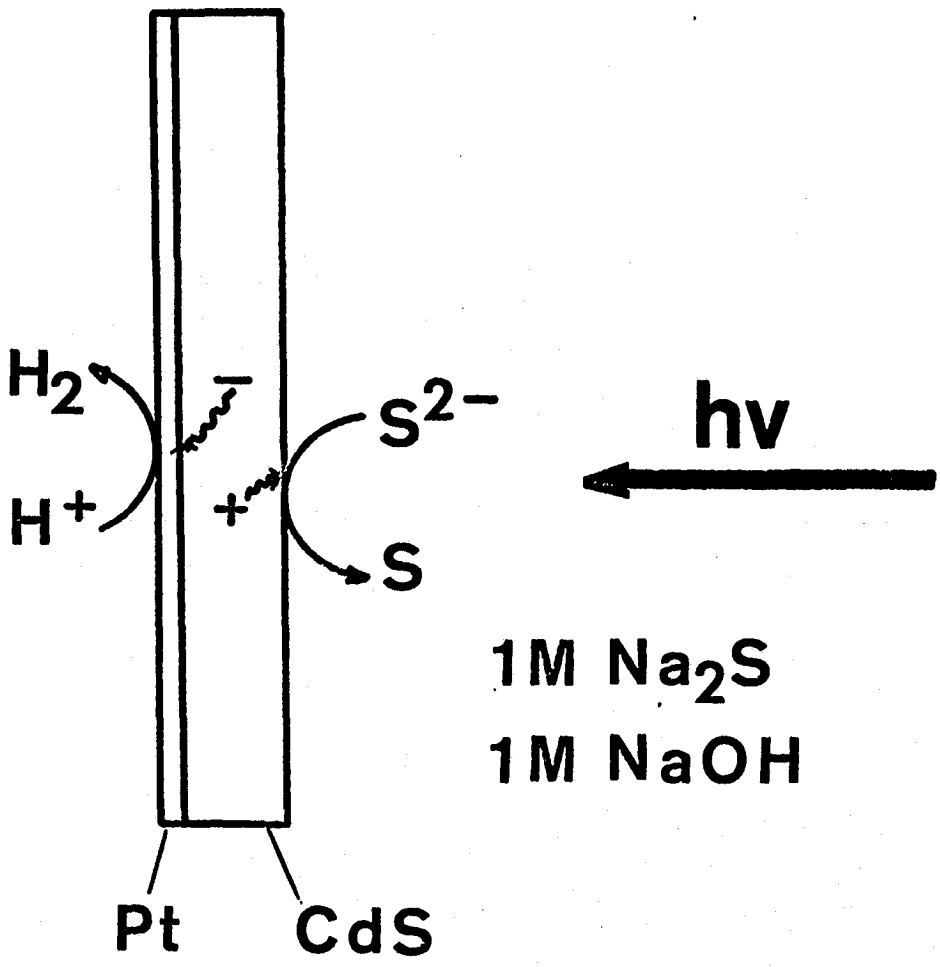

Fig. 17: Operation of Pt/CdS photoelectrochemical diode.

in 4:1 HCl/HNO_3, then in 1M NaCN to dissolve excess S, and finally rinsed with H_2O. The crystal was placed on a glass slide on a hot plate heated to ∿300°C. The hot top surface of the crystal was then coated with an aqueous solution of 5% H_2PtCl_6. Pyrolysis of the latter resulted in an even black deposit of Pt.

A qualitative assessment of the diode activity was made by sealing it in vacuo in a pyrex tube containing the aqueous Na_2S electrolyte. The latter was subjected to several degassing cycles to remove dissolved O_2. Diodes prepared in this way showed vigorous H_2 evolution under irradiation with light of λ <500 nm, the CdS band gap. The photoelectrochemical gas evolution was demonstrated to be continuous over 3-4 hours. Storage of the sealed tubes for more than a month has led to no diminishing of the diodes' activity. The diodes were also active at atmospheric pressure under N_2 or Ar.

Although longer term tests remain to be completed, several possibilities exist for ultimate failure of these diodes. Some deplatinization has been observed during operation of the diode, which indicates that more adherent deposits must be produced. In addition, eventually the S_n^{2-} concentration will increase to a point where its reduction will compete with H_2 evolution. Finally, although no evidence has yet been found, the CdS surface may become etched over the long term, with a concurrent decrease in photoresponse.

Several attempts to observe H_2 evolution with platinized CdS powder also sealed in vacuo with the Na_2S electrolyte led to inferior results. Apparently the high electrical quality of the single crystal is required for producing active diodes.

These diodes may be employed in making H_2 in the presence of a sacrificial redox species such as S^{2-}, I^-, $Fe(CN)_6^{4+}$, etc. The second half of the H_2O decomposition could then be carried out either electrochemically or photoelectrochemically, viz.

$$ox + H_2O \rightarrow red + O_2 \qquad E° < 1.23V \tag{5}$$

Alternatively, the H_2 could be used with the oxidized species in an electricity-generating fuel, i.e.,

$$ox + H_2 \rightarrow red + H^+ + \text{electricity} \tag{6}$$

CdS photodiodes were also evaluated in a particulate configuration, as described above. Cadmium sulfide particles were partially platinized using the photodeposition method. In a neutral aqueous solution containing 1M NaI, the photoinduced evolution of H_2 was vigorous. However, fatiguing occurred within 2 hours, similar to that noted for n-$SrTiO_3$.

IV. p-TYPE PHOTOCATHODES

Considerable disagreement exists in the literature regarding flat band potentials of p-type semiconductors. Figure 18 gives the positions of E_C and E_V of some of these materials using an average of literature values. It is evident that GaP, CdTe and InP are marginally Class I semiconductors. Their valence bands lie very close to the O_2/H_2O potential. However, in a single photoelectrode configuration, the anode could be of a state-of-the-art O_2 electrode, minimizing the overpotential for that reaction.

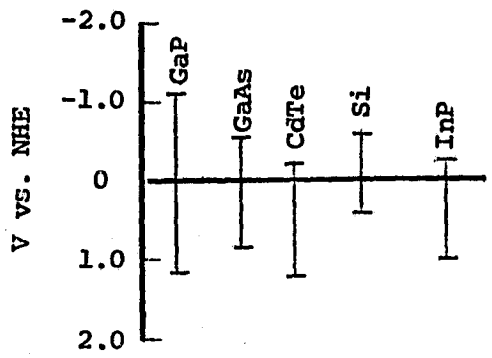

Fig. 18: Band energetics of some p-type photocathodes at pH 1.

A. p-GaAs

As a model system, we have evaluated the photoelectrochemical properties of p-GaAs. Single crystals were oriented along the 111 plane, were Zn doped, and of ∿0.15 Ω-cm resistivity. Crystals were polished with diamond paste, then chemically etched with concentrated H_2SO_4:30% H_2O_2:H_2O (3:1:1) for 15 seconds, followed by 15 seconds in 6M HCl. The crystal was then rinsed with distilled H_2O before use.

Current voltage curves for p-GaAs in pH 1 electrolyte are shown in Figure 19 in the dark and under chopped illumination. Both anodic and cathodic dark currents were observed. The anodic current should be due to Ga^{+3} dissolution and to Ga_2O_3 formation. The latter process has been employed in GaAs device technology, and is known to occur with the simultaneous formation of elemental Ar.

The onset of anodic current occurs at ∿+0.2V vs. SCE. Fan and Bard (21) have placed the position of the valence band of GaAs at pH 0

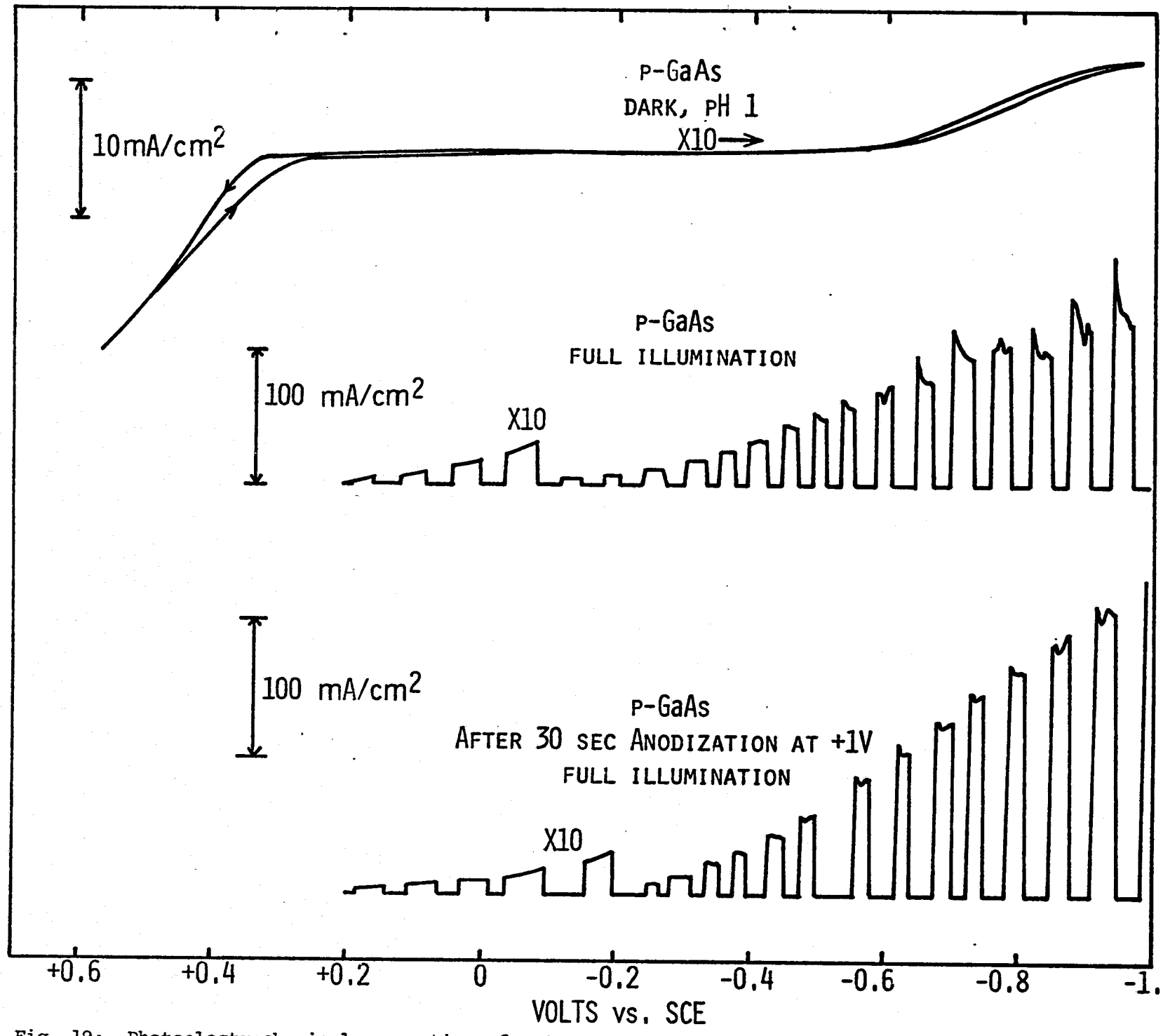

Fig. 19: Photoelectrochemical properties of p-GaAs under chopped illumination of a 150W Xe light source, in pH 1 aqueous electrolyte.

at +0.75V vs. SCE. The onset of anodic current negative of this potential may be ascribed to a tunneling of holes from the valence band through an intermediate surface state. The cathodic dark current occurs at a potential where the bands are bent to such a high degree that they are nearly degenerate. This condition leaves open the possibility of tunneling of electrons from the valence to conduction band, from which H_2 evolution can occur.

In the light, the crystal gave one of the largest photoresponses yet observed, with photocurrents of $\sim$100 mA/cm^2 being developed under high negative bias using the full output of the Xe light source. However, the onset of photocurrent is only $\sim$100-200 mV positive of the thermodynamic H_2 evolution potential, so the net energy storage is rather small. Fan and Bard have noted photoreduction of Eu(III) (E° = -0.67V vs. SCE) p-GaAs under similar conditions, so that the slower H_2 evolution may be a problem of high kinetic overpotential for that reaction on GaAs. Preliminary attempts were made to adsorb Pd and Ru on the p-GaAs surface by dipping the freshly etched crystal in an aqueous solution of the metal nitrate as chloride containing 0.1M HNO_3 (22). It was hoped that this would provide catalytic sites for H_2 evolution. Both treatments, however, led only to net reductions in photocurrent. A dramatic increase in photocurrent was noted if the p-GaAs was initially anodized at +1V vs. SCE. The surface oxide thus formed may have the effect of suppressing surface recombination, an effect well known in MIS device technology.

A longer term stability test was carried out for the p-GaAs photocathode. The crystal was first anodized at +1V for 30 seconds in the dark, then illuminated with the full intensity of the Xe lamp at a bias of -1V vs. SCE. The H_2 generated during photoelectrolysis was collected, and compared to the photocurrent passed over 2 hours. Within $\pm$ 2% accuracy of the apparatus, the H_2 evolution current efficiency was 100%. As shown in Figure 20, the photocurrent decreased from 200 mA/cm^2 to $\sim$25 mA/cm^2 during the course of the experiment. Atomic absorption analysis of the electrolyte revealed a small amount of As, which would account for 0.1% of the total current. At pH 1, we calculate the potential of AsH_3 formation to be $\sim$-0.75V vs. SCE, near the flat band potential. Hence, AsH_3 formation is probably thermodynamically feasible for photogenerated electrons in p-GaAs, but both thermodynamics and kinetics favor H_2 evolution.

B. p-CdTe

In addition to p-GaAs, a preliminary evaluation of p-CdTe was undertaken. Twinned crystals were obtained from Cleveland Crystals, and were 0.7 cm in diameter x 0.1 cm thick, with a resistivity of $\sim 10^4 \Omega$-cm. Apparently it is difficult to prepare low resistivity p-type samples by the conventional defect doping process. A thermopower measurement confirmed the p-doping of the samples.

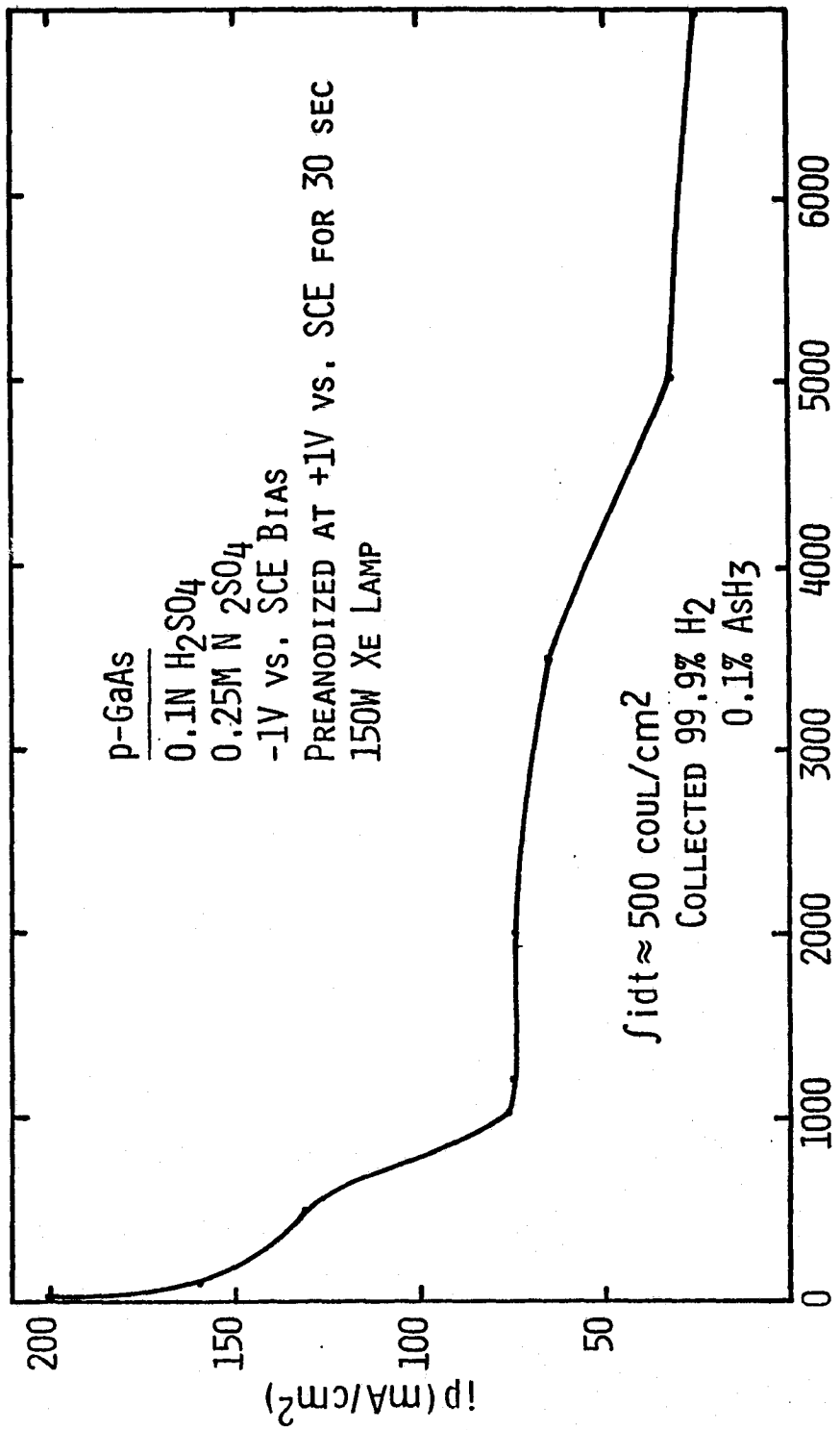

Fig. 20: H_2 evolution photocurrent as a function of time for p-GaAs. The electrode was held at -1V vs. SCE in a pH 1 aqueous electrolyte.

The photocurrent-voltage curve for p-CdTe in pH 1 aqueous electrolyte is shown in Figure 21. The very light doping of the crystal is indicated by the photoresponse in both directions, indicating that the Fermi level is near mid-gap rather than near the band gap. The p-type response appeared to increase with repeated scans out to -2V vs. SCE.

The onset of cathodic photocurrent is rather negative because of the light sample doping (see Figure 22). Because of the undermined (and large) separation between the conduction band and the Fermi level, the onset of photocurrent cannot be used to accurately map the band energetics. The energetics indicated in Figure 22 are obtained from more heavily doped n-type samples.

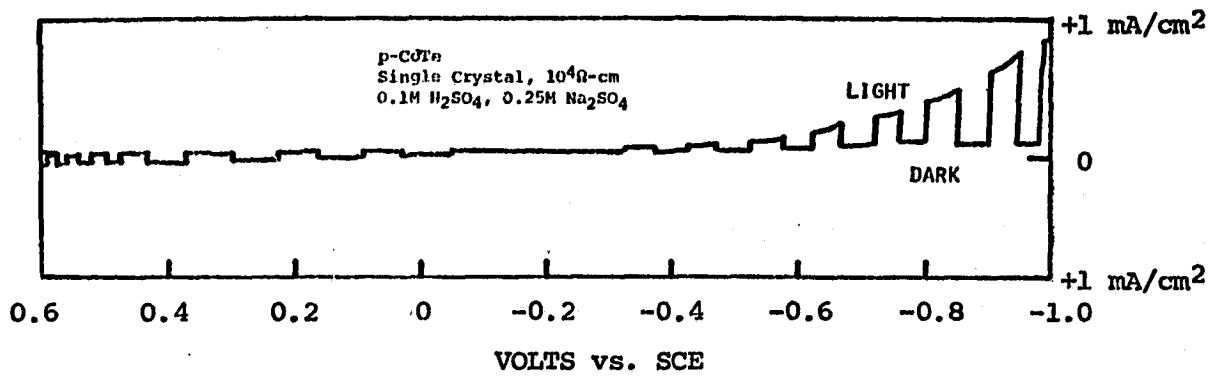

Fig. 21: Current-voltage curve for p-CdTe in the dark and under full illumination of a 150W Xe lamp.

Holding the voltage at -2V for 30 minutes resulted in a steady photocurrent with no apparent deterioration of the crystal surface. Thus, if p-CdTe becomes available with heavier doping, a robust Class II photocathode may be possible.

C. Other Photocathodes

Two new potential photocathodes have been synthesized, p-WSe_2 and p-$ZnSiAs_2$. WSe_2 has been reported by Gobrecht and co-workers (23) to be a highly robust photoelectrode. The WSe_2, which has a layer structure, was produced by the direct reaction of the elements in a sealed, evacuated quartz tube, at 550°C for 3 days, then at 1050°C for 8 hours, followed by slow cooling. The resulting compound was pressed into a pellet at 9000 psi for ~45 seconds. As is typical of these layered materials, relatively strong pellets could be produced by this procedure. Using the 4-point probe technique, resistivities of the WSe_2 pellets ranged from 50-100 Ω-cm.

Prior to mounting, electrodes were soaked in a 10% NaCN solution to remove excess Se, then rinsed with distilled water. Evaluation of the electrodes in a pH 10 borate buffer revealed a weak, p-type photoresponse

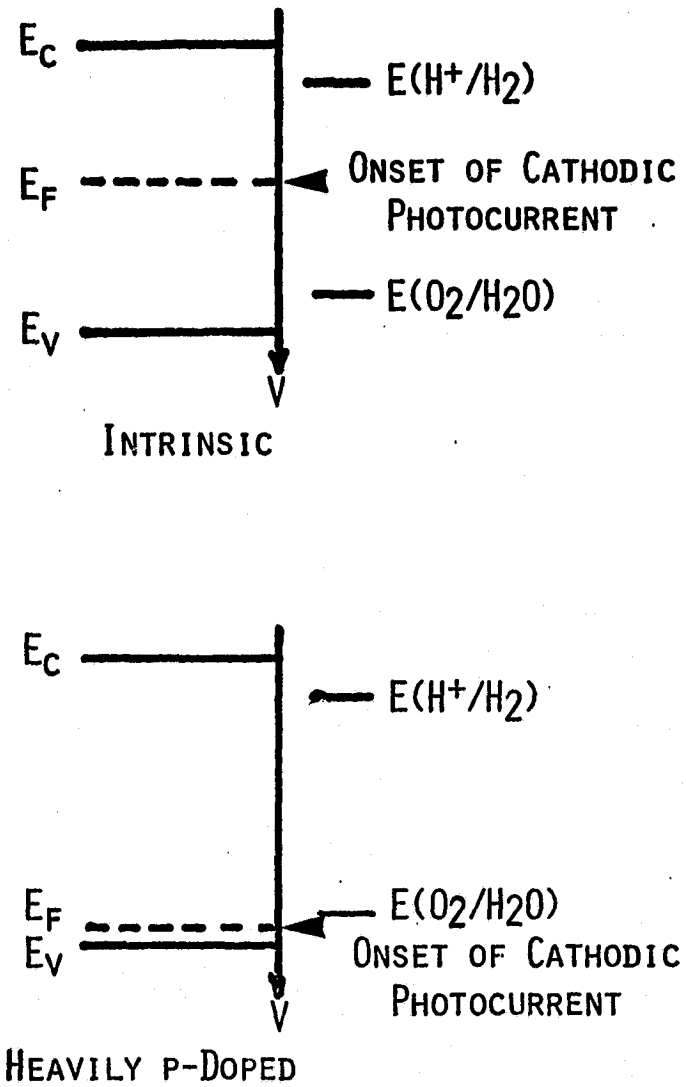

Fig. 22: Onset of cathodic photocurrent in intrinsic and heavily p-doped CdTe.

in all cases. We concluded that further measurements should be made in single crystalline electrodes. Very recent work on WSe_2 photoelectrochemistry indicates that certain faces of WSe_2 are degenerate, leading to many short circuits and hence poor photoresponse in polycrystalline electrodes (24).

A synthesis of $ZnSiAs_2$ was carried out, also from the elements at elevated temperature in a sealed quartz tube. The chalcopyrite structure was identified by X-ray diffraction analysis. A polycrystalline sample taken directly from the reaction tube was mounted as a photoelectrode. Again, the response in pH 10 borate buffer was weakly p-type. Further work will entail evaluation of thin evaporated films of this material.

V. SYSTEMS CONSIDERATION

A. Photochemical and Photoelectrochemical Solar Energy Conversion

Photoelectrolysis is a quantum process for solar energy conversion. In this way, it is related to other photochemical conversion schemes such as norbornadiene photoisomerization (25), photosensitized splitting of water by dissolved Ir and Ru complexes (26), and the production of electricity using photovoltaic cells. Unlike solar thermal conversion, such quantum processes can never make use of 100% of the solar spectrum because of the wavelength dependence of the electronic transitions characterizing the absorbing species. However, photochemical conversion of solar energy has several distinct advantages over thermal processes:

- Fuel with a high molar energy content can be produced at ambient temperature. Collectors, therefore, need no insulation.
- Fuel production rates are dependent only on the total photon flux in the appropriate wavelength range. These rates are not dependent on the outside temperature or the relative diffuseness of the light (for nonfocusing collectors).

The thermodynamics of endoergic photochemical reactions has recently been considered by several authors (27-29), allowing us to predict optimal rates and efficiencies of solar fuel production. These calculations relate to reactions of the general form:

$$A + nh\nu \rightarrow B \qquad (7)$$

$$B \rightarrow A + \text{heat} \qquad (8)$$

These theoretical considerations (which have little experimental verification) estimate that the minimal sum of photon energies required to promote reaction (7), either directly or by sensitization, must be 0.4 to 0.8 eV greater than $\Delta G_{B \rightarrow A}$. We have used the more conservative 0.8 eV "loss factor," as was also employed by Bolton (27) in order to compute minimum wavelengths for promoting certain fuel forming reactions, if the appropriate sensitizers can be found. For a 2-photon water splitting reaction, typified by a single photoelectrode photoelectrolysis cell, this minimum wavelength is 611 nm. Under AM1 insolation, the solar photon flux below 611 nm is 7.52 Einsteins/m^2-hr. If the quantum yield for the reaction is 1.0, the storage rate is 1075 kJ/m^2-hr, if the H_2 is

is used as heat. This represents a 30% conversion of solar energy to H_2. Similar data for other photochemical fuel-forming reactions are presented in Table 12.

Nozik (30) has presented a simple framework for considering the economics of photoelectrolysis of water. He assumes a total absorbed solar power of 2000 kWh/m^2-yr, typical of a nontracking collector in the Southwestern U.S. If this sunlight were used at 100% efficiency, it would produce H_2 equivalent to 6.86M BTU/m^2-yr. If CC is the capital cost per m^2 of the collector, and mortgage and upkeep of the collector amounts to 20% of CC/yr, then the cost of the H_2 produced is

$$\text{Cost (\$1M BTU)} = \frac{CC(0.2)(100)}{6.8\,\alpha} \qquad (9)$$

where α is the solar conversion efficiency. In Figure 23, costs of H_2 are plotted vs. efficiency for collectors of different capital cost. Figure 23 shows that with an optimized system of 30% conversion efficiency, and collector costs of \$10-\$50/m^2, H_2 costing \$1-\$5/M BTU could be obtained.

What are the prospects regarding actual collector costs in such photochemical systems? Since there is no need for insulation, only a shallow tray is necessary to contain the water and active elements. Additionally, H_2 must be given off in a restricted area to allow its collection, so a plastic cover may be required. If a particulate semiconductor system is used, an H_2/O_2 mixture would be evolved off of each grain. This would be the least costly configuration, e.g., a 0.1 mm x 1 m^2 layer of TiO_2 costs $\sim$\$5/m^2 based on today's prices. Hence, \$10/m^2 is a realistic estimate for a simple photochemical collector as installed. A collector with photoelectrodes, where H_2 could be easily separated from O_2, would cost somewhat more depending on the configuration and materials.

B. 4-Photon Water Decomposition System

A 2-step process for the photoelectrochemical decomposition of water using visible light and using "state-of-the-art" photoelectrodes. This is accomplished by an intermediate redox storage reaction. For example, in the case of n-CdS and n-Fe_2O_3, water could be decomposed spontaneously using cells 1 and 2 below:

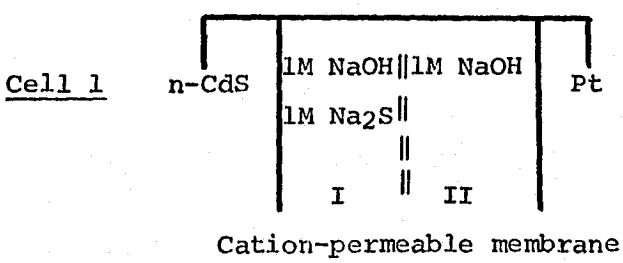

Cation-permeable membrane

TABLE 12

OPTIMAL RATES OF PHOTOCHEMICAL ENERGY STORAGE UNDER AM1 INSOLATION ASSUMING A MAXIMUM λ CORRESPONDING TO $\Delta G_{reaction}$ + 0.8 eV. A THERMAL ENERGY STORAGE SYSTEM IS INCLUDED FOR COMPARISON.

REACTION	N	ΔH (KJ/MOLE)	λ (NM)	N(Δλ) (EIN/M² HR)	STORAGE RATE (AM1) (KJ/M² HR)
$H_2O \rightarrow H_2 + \frac{1}{2} O_2$	2	286	611	7.52	1075
$CO_2 + H_2O \rightarrow HCOOH + 1/2\ O_2$	2	270	543	5.79	782
$CO_2 + 2H_2O \rightarrow CH_3OH + 3/2\ O_2$	6	727	576	6.75	818
$N_2 + 3H_2O \rightarrow 2NH_3 + 3/2\ O_2$	6	765	629	8.18	1043
$CO_2 + H_2O \rightarrow 1/6\ C_6H_{12}O_6 + O_2$	4	467	607	7.46	871
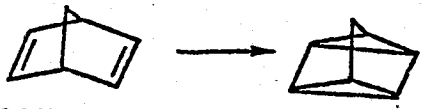	1	112	621	7.94	889
20% SOLAR CELL PLUS ELECTROLYZER	1	→			720 η_{EL}
30% MULTIJUNCTION SOLAR CELL PLUS ELECTROLYZER	1	→			1080 η_{EL}
THERMAL STORAGE	-	107	FULL SUN	-	1800
$CaCl_2 \cdot 2MeOH \rightarrow CaCl_2 + 2MeOH$		(ΔS = 0.25 KJ/MOLE-DEG)			(50% COLLECTOR EFFICIENCY)

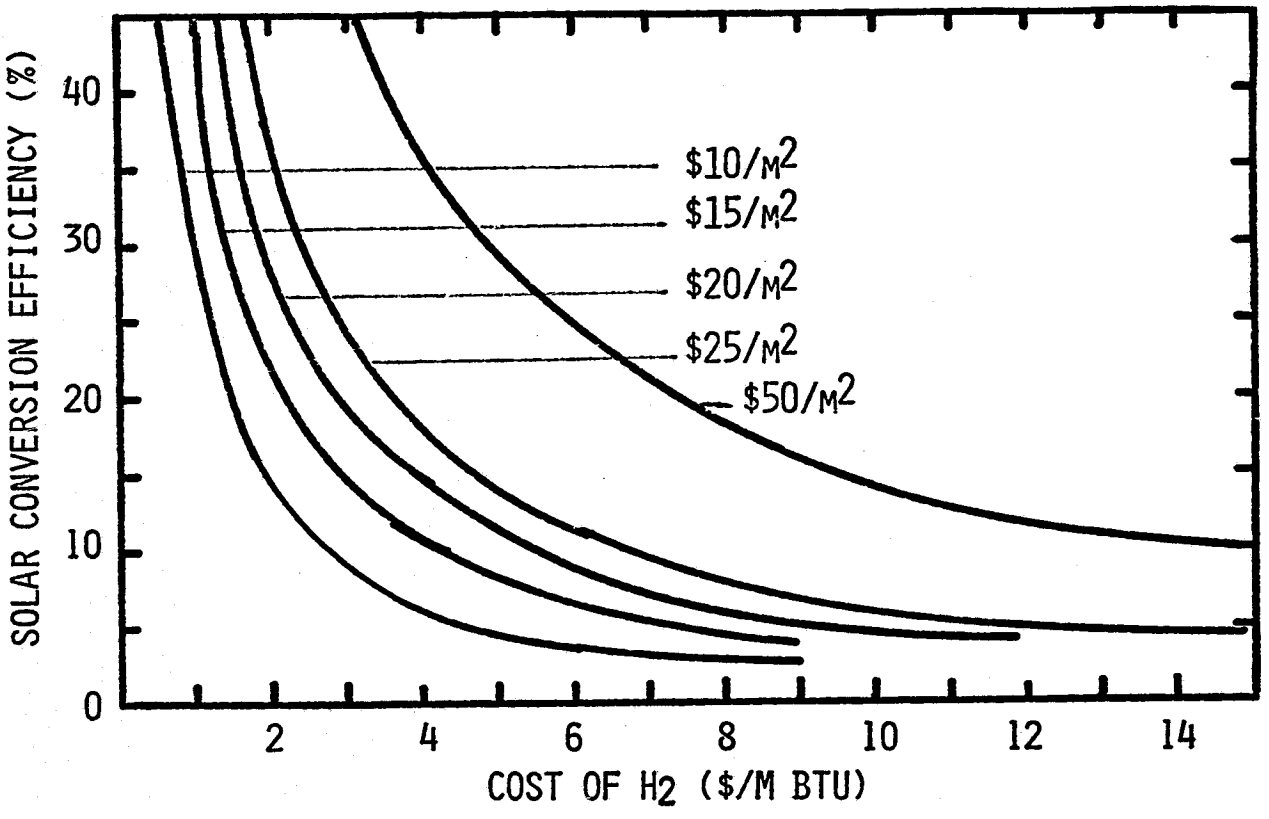

Fig. 23: Cost of H_2 produced by solar photoelectrolysis of water, as a function of solar conversion efficiency and collector cost (after Nozik, Ref. (30)).

Reactions: $S^{2-} \xrightarrow[h\nu]{CdS} S + 2e^-$ (redox storage and corrosion suppression)

$$2e^- + 2H_2O \xrightarrow{Pt} H_2 + 2OH^-$$

Cell 2

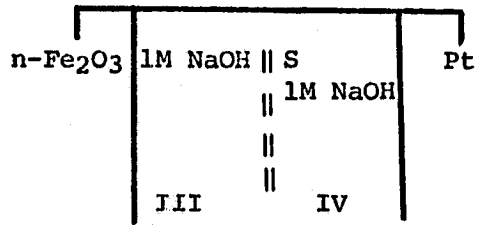

Reactions: $H_2O \xrightarrow[h\nu]{Fe_2O_3} 2H^+ + \frac{1}{2}O_2 + 2e^-$

$$2e^- + S \xrightarrow{Pt} S^{2-}$$

Thus, with two separate cells and exchange of electrolyte between II and III and between I and IV, a cyclic process is achieved.

Reflection on these two tandem cells indicate that they are equivalent to an electrochemical photovoltaic cell of configuration

$$CdS|1M\ NaOH,\ S_n^{2-}|Pt$$

boosting an Fe_2O_3 photoelectrolysis cell:

$$Fe_2O_3|1M\ NaOH|Pt$$

Thus, either configuration could be employed in a practical system.

We constructed and tested such a dual photoelectrode cell using two rectangular glass cuvettes (Figure 24a). The CdS (0.5 Ω-cm, Cleveland Crystals) and Fe_2O_3 (sintered disc, 1% TiO_2) were mounted in a glass rod with a Ni lead using Ag epoxy for the contact. The CdS/Pt cell contained 1.0M Na_2S, 1.0M S and 1.0M NaOH. The Fe_2O_3/Pt cell was 0.25M Na_2SO_4, 0.1M H_3BO_3, adjusted to pH 10. Since the CdS/Pt cell is biasing the Fe_2O_3/Pt cell, the electrodes were connected as in Figure 24b. The i-V curves of the tandem pair in the dark and under illumination are shown in Figure 25. It can be seen from Figure 25 that the 4-photon process can be driven only with light absorbed by the semiconductors, and needs no external bias.

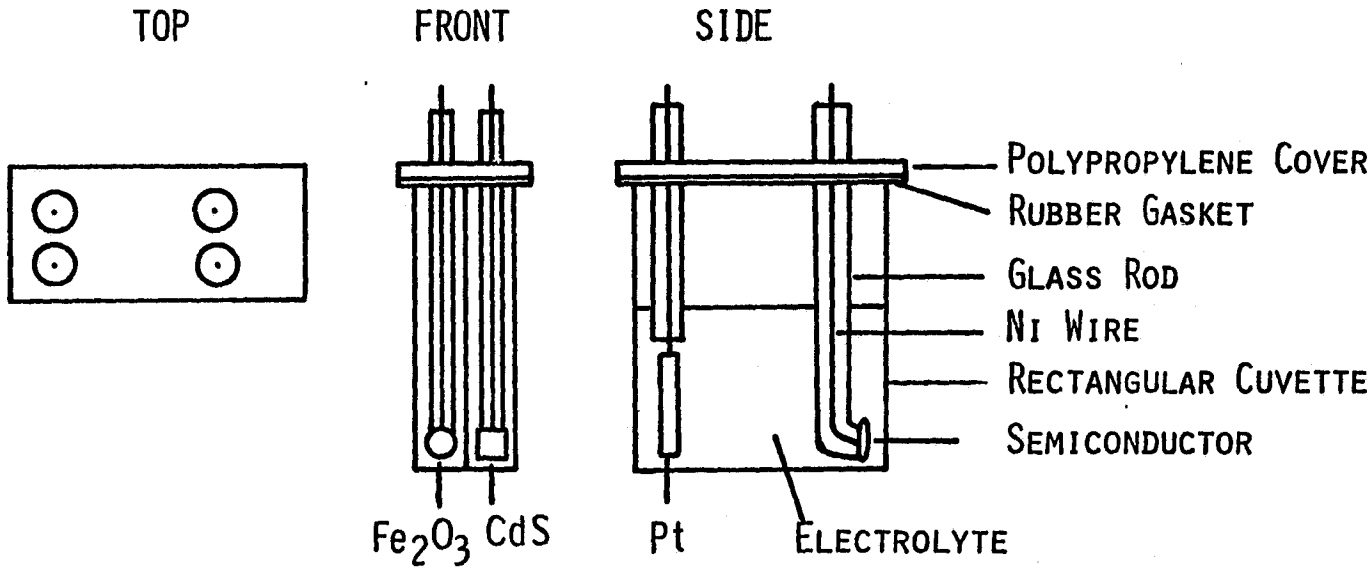

(a) Experimental configuration for a two-stage water photoelectrolysis cell.

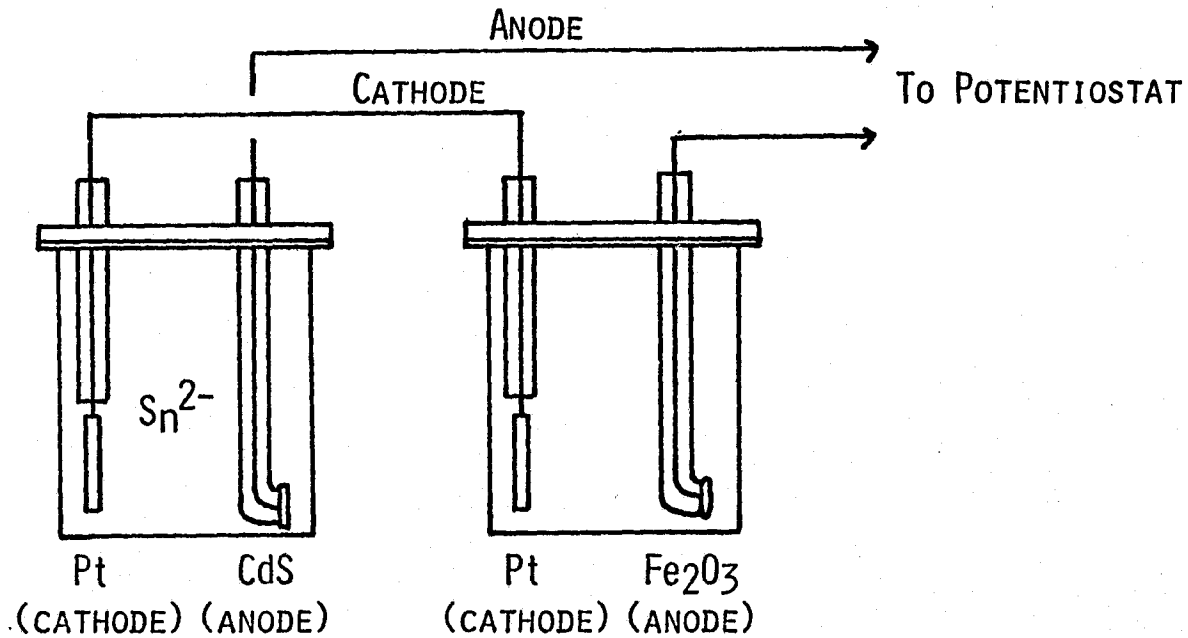

(b) Series connection of photoelectrochemical cells. Consder the CdS/Pt cell as a battery biasing the Fe_2O_3/Pt water electrolysis cell; the potentiostat adds an additional bias.

Fig. 24: Cells for 4-photon photoelectrochemical H_2O decomposition.

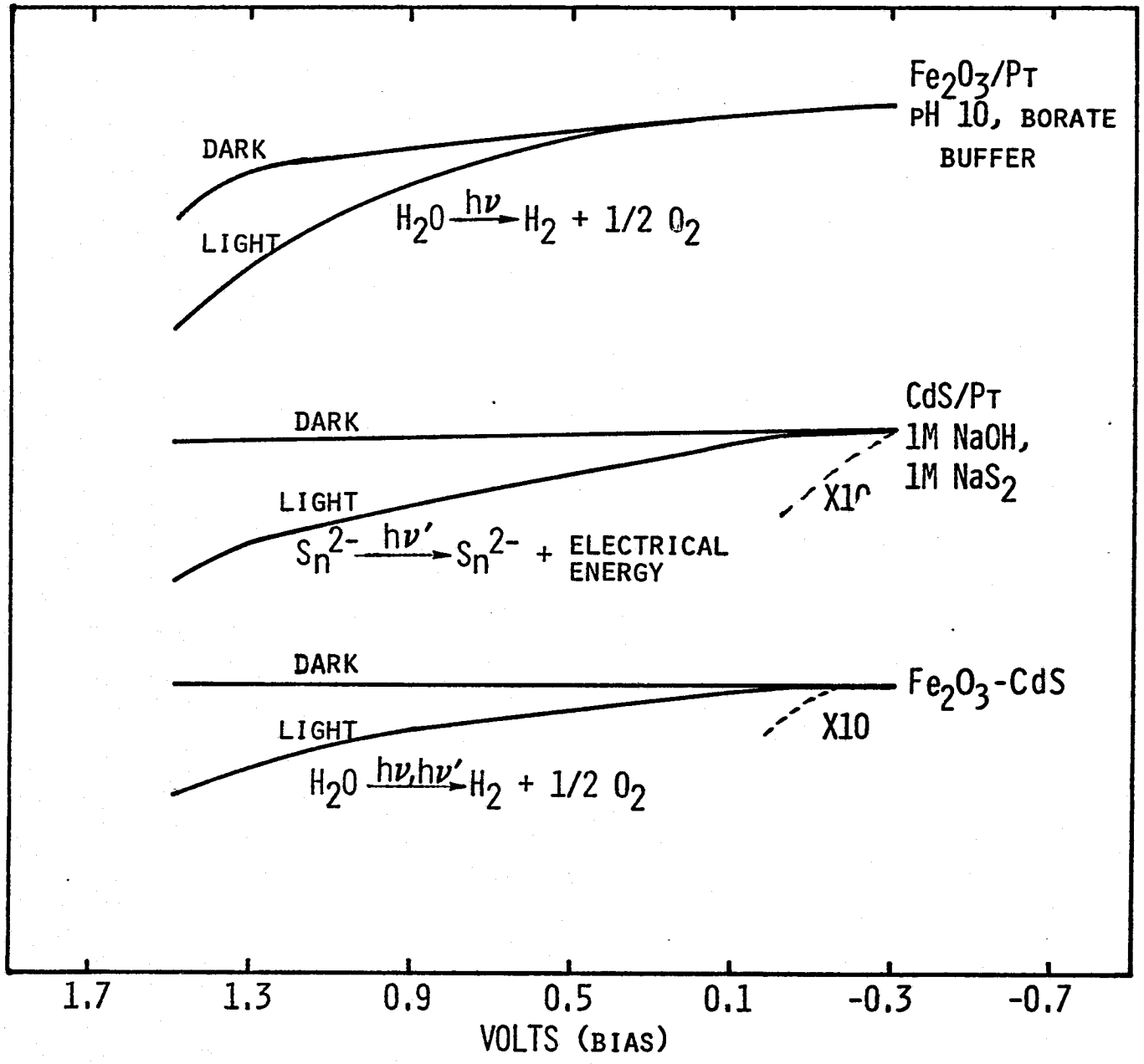

Fig. 25: Dark and light curves for separated and tandem photoelectrolysis cells as a function of bias voltage. Irradiation with Xe arc, ~100 mW/cm^2.

These kinds of photoelectrolysis are, in principle, highly economical. They can employ very inexpensive thin film electrodes, such as chemically deposited Cd chalcogenides or Fe_2O_3, and thus have a distinct advantage over solid state solar cells in conjunction with a water electrolysis cell.

Toward this end, we have begun investigating the pyrolysis of Cd thiourea complexes as a means of electrode fabrication. Numerous thin film electrodes were produced using a solution of 0.05M thiourea, 0.025M $CdCl_2$ in MeOH. Initial attempts were made on glass substrates which had been thoroughly degreased and freed of alkali metal ions by washing at 80°C with chromic acid. These were dip or spray coated with the MeOH solution, then placed in a 75°C oven to dry, leaving behind a film of the thiourea complex. Pyrolysis of the thiourea complex at 400-500°C left behind the desired CdS film.

We soon determined that films of equal or better quality could be produced by dipping the substrates, followed by placing them in a flame. This procedure worked especially well for metallic substrates. Films were prepared by multiple dipping-flaming on Ni, stainless steel, Pt and Mo. On the latter, oxidation of the base metal appeared to be the dominant process, while on the other three, relatively uniform films of CdS were produced. Photoelectrochemical evaluation of these films in 1M Na_2S, 1M NaOH revealed by far the highest activity using the Pt substrate. In this case, the photoeffect was nearly as large as that of a CdS single crystal, which was tested in a parallel study. The formation of an intermediate layer of the parent metal oxide may interfere with the photoresponse on stainless steel or Ni.

VI. SUMMARY AND CONCLUSIONS

During the last two years, our primary efforts on this program have been directed toward the problem of photoanode development. As outlined in Section I, this has evolved into a search for low electron affinity oxides with band gaps below 2.5 eV. The following conclusions are possible based on our accumulated results:

- The best Class I photoanode yet discovered is $SrTiO_3$ (ΔE_g = 3.1 eV). No Class I oxide with ΔE_g <3 eV has yet been found, although some sensitization of TiO_2 (nearly a Class I material) to the visible spectrum has been achieved with d^n metal substitution or, in other work, through the effect of surface-adsorbed dye molecules.

- The best Class II photoanodes are Fe_2O_3 (ΔE_g = 2.1 eV) and $Fe_{2-x}Rh_xO_3$ (ΔE_g = 1.5-2 eV). These materials require an external bias of >0.5V to effect complete photoelectrochemical H_2O decomposition. The presence of Rh appears to enhance the photoresponse via sensitization to lower energy light, without adversely affecting the flat band potential. The external bias could be supplied by a suitably matched p-type semiconductor (e.g., p-CdTe).

- The kinetics of electron transfer for water oxidation appear to be enhanced by the mediation of CO_3^{2-} oxidation, in the cases of Fe_2O_3 and Rh-substituted Fe_2O_3. Similar effects have been observed by Gerstner et al. (3) with SO_4^{2-} at TiO_2 electrodes. Thus, it is possible that the efficiency of sunlight utilization in the water oxidation reaction can be increased by varying the composition of the solution.

- The d-band oxide PdO is potentially a superior Class II photoanode, with V_{fb} $\sim$0.3-0.4V vs. NHE and $\Delta E_g \approx$1.5 eV (1,7,8). Films of PdO formed by thermal oxidation of the parent metal tend to be p-type, although some n-type specimens were obtained and tested. Since the PdO valence band is of d-electron origin, it does not lie as deeply in energy as a valence band derived mostly from the oxygen (2p) bonding orbital.

- Only limited success has been achieved so far with d^n/d^o mixed metal oxides (1,2). The d^n cation sublattice only exhibits partial band formation in most examples tried, the cations often acting as traps for electron and holes and diminishing the overall photoresponse. However, several examples were noted of d^o, large gap insulators exhibiting visible light photoresponse on the introduction of d^n ions into the lattice.

- p-type photocathodes exist which show good stability under conditions of H_2 evolution, among them p-CdTe, p-GaP, and p-GaAs. In general, photovoltages are not as large as for n-type materials, a condition which may result from the presence of a high density of surface states.

- The economics of photoelectrolysis has been addressed, and potentially inexpensive systems have been specified for development. These include 1) particulate suspensions of semiconductor particles or diodes and 2) a 4-photon water decomposition with intermediate redox storage. These concepts were demonstrated for systems based on platinized $SrTiO_3$ (H_2O decomposition), platinized CdS (H_2S decomposition) and a CdS/Fe_2O_3 dual photoelectrode cell.

Based on these results, areas for further investigation can be delineated, with the goal of producing H_2 and, ideally, O_2 efficiently and economically using sunlight. Considerable fundamental research is still required to bring photoelectrolysis of water into the "interesting" stage for solar energy conversion, i.e., >5% efficient. Key developments in d-band oxide photoanodes are necessary, both in their doping and transport properties. Photocathodes such as p-CdTe and p-WSe_2, which appear to be stable under H_2 evolution, must still have their surface properties controlled so that a good liquid junction can be formed. Finally, those photoelectrolysis systems must be stressed which make use of their advantages over the electrolysis of water using the output of conventional solar cells. These systems would be based on photoelectrochemical diodes or thin film electrodes, and would take advantage of the ease of formation of the liquid junction.

VII. REFERENCES

1. R. D. Rauh, S. A. Alkaitis, J. M. Buzby and T. F. Reise, Final Report, Contract EC-77-C-01-5060, U.S. Department of Energy, March, 1979.

2. R. D. Rauh, J. M. Buzby, T. F. Reise and S. A. Alkaitis, J. Phys. Chem., 83, 2221 (1979).

3. L. A. Hanis, D. R. Cross and M. E. Gerstner, J. Electrochem. Soc., 124, 839 (1977); M. E. Gerstner, ibid., 126, 944 (1979).

4. J. M. D. Coey and G. A. Sawatzky, J. Phys., 4C, 2386 (1971).

5. G. Bayer and H. G. Wiedemann, Thermochim. Acta, 15, 213 (1976).

6. A. Wold, R. J. Arnott and W. J. Croft, Inorg. Chem., 2, 972 (1963).

7. M. A. Butler, J. Appl. Phys., 48, 1914 (1977).

8. L. Katz and R. Ward, Inorg. Chem., 3, 205 (1964).

9. B. Matthias, Phys. Rev., 73, 808 (1948).

10. J. Dickson, L. Katz and R. Ward, Inorg. Chem., 10, 713 (1961).

11. A. K. Ghosh and H. P. Maruska, J. Electrochem. Soc., 124, 1516 (1977).

12. A. L. Allred and E. G. Rochow, J. Inorg. Nucl. Chem., 5, 264 (1958).

13. J. B. Goodenough, Progr. Sol. State Chem., 5, 145 (1972).

14. J. P. Hoare, The Electrochemistry of Oxygen (New York: Interscience, 1968).

15. A. C. C. Tseung and S. Jasem, Electrochim. Acta, 22, 31 (1977).

16. R. Scheerer and M. Grätzel, Ber. Bunsenges. Phys. Chem., 80, 979 (1976).

17. C. D. Jaeger and A. J. Bard, J. Phys. Chem., 83, 3146 (1979).

18. V. O. Schmitz-DuMont and H. Kasper, Z. Anorg. Chem., 341, 252 (1965).

19. B. Kraeutler and A. Bard, J. Am. Chem. Soc., 100, 4317 (1978).

20. M. S. Wrighton, P. T. Wolczanski and A. B. Ellis, J. Solid State Chem., 22, 17 (1977).

21. F. F. Fan and A. J. Bard, J. Am. Chem. Soc., in press.

22. B. Parkinson, A. Heller and B. Miller, J. Electrochem. Soc., 126, 954 (1979).

23. J. Gobrecht, H. Gerischer and H. Tributsch, Ber. Bunsenges. Phys. Chem., 82, 1331 (1978).

24. T. E. Furtak and B. A. Parkinson, First Quarterly Technical Progress Report, Subcontract XP-9-8198-1, February, 1980; W. Kantek, H. Gerischer and H. Tributsch, Ber. Bunsenges. Phys. Chem., 83, 1000 (1979).

25. P. S. Mariano and T. L. Rose, "Hydrocarbon Entrapment of Light Energy of the Sun," Final Report, Department of Energy, Division of Energy Storage Systems, Contract No. EC-77-G-05-5621, December, 1978; C. Kutal et al., 2nd Int. Conf. Photochem. Conver. Energy Storage, Cambridge, England, August 10-12, 1978, p. 7; G. Jones, II, S-H. Chiang and P. T. Xuan, J. Photochem., 10, 1 (1979).

26. G. L. Geoffrey, G. S. Hammond and H. B. Gray, J. Am. Chem. Soc., 97, 3933 (1975); N. Sutin, J. Photochem., 10, 19 (1979).

27. J. R. Bolton, Science, 202, 705 (1978).

28. R. T. Ross and T. L. Hsiao, J. Appl. Phys., 48, 4783 (1977).

29. A. W. H.-Mau and W. H. F. Sasse, Proc. Roy. Aust. Chem. Instit., CSIRO, 44, 89 (1977).

30. A. J. Nozik, Proc. 11th IECEC, Lake Tahoe, Nevada (1976).